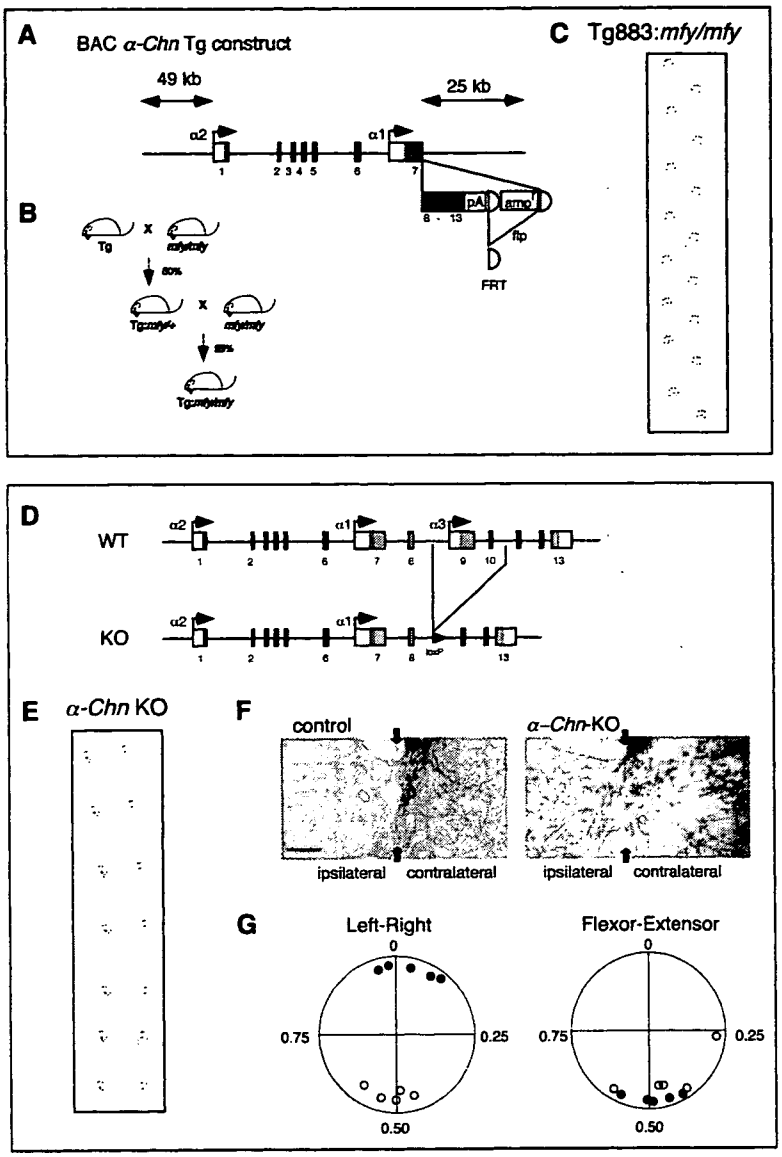


**Figure 4. Disruption of *α-Chn* Is Responsible for the *mfy* Phenotypes**

(A) Schematic of the BAC Tg construct. A cDNA fragment containing exons 8–13, a poly(A) signal, and an *amp*$^r$ selection marker flanked by two FRT sites was inserted immediately after exon 7 of a BAC clone covering exons 1–7 of *α-Chn*, using Red/ET homologous recombination in bacteria. *Amp*$^r$ was removed from the BAC construct by expressing flp recombinase in the bacterial clone.

(B) Tg mouse lines were generated by injecting the linearized construct into fertilized mouse eggs. Two lines of Tg mice were crossed with *mfy/mfy* mice to yield Tg:*mfy*/+ mice. These were then crossed with *mfy/mfy* mice to obtain Tg mice in a *mfy/mfy* background.

(C) Improved walking of Tg#883:*mfy/mfy* mice. All Tg#883:*mfy/mfy* mice showed a marked improvement in the control of walking.

(D) Schematic of the KO allele, in which exons 9 and 10 were deleted by homologous recombination in ES cells, and Cre/loxP recombination in the mouse germline.

(E) Representative hind-limb footprint patterns of *α-Chn* KO mice showing a hopping gait similar to that of *mfy/mfy* mice.

(F) Anterograde tracing of CST axons and sectioning at cervical levels of the spinal cord. CST axons of *α-Chn* KO mice aberrantly recrossed the spinal cord midline, as seen in *mfy/mfy* mice. Scale bar: 100 μm.

(G) Circular phase diagrams for the locomotor-like activity of five control (open circles) and five *α-Chn* KO (filled circles) mice at P1–P3. Left-right VR activity in the lumber spinal cord of *α-Chn* KO mice was synchronous as that of *mfy/mfy* mice.

as a downstream mediator of ephrinB3/EphA4 forward signaling in developing CST axons.

### Interaction between α-Chimerin and EphA4

To test whether α-chimerin interacts with EphA4, we co-transfected 293T cells with *EphA4* and *α-Chn*-expression constructs and immunoprecipitated EphA4 from cell lysates with Fc region-fused ephrinA1. Both α1-chimerin and α2-chimerin were precipitated with EphA4$^{WT}$ and kinase-dead EphA4$^{FF}$ (Figure 5A), and α2-chimerin$^{mfy}$ was also precipitated with EphA4 (Figure S9). These results suggest that α-chimerin interacts with EphA4 in vitro and that this interaction does not require the kinase activity of EphA4 or the GAP activity of α-chimerin. To identify the region of α-chimerin responsible for interacting with EphA4, we performed an in vitro glutathione S-transferase (GST) fusion protein pull-down assay. EphA4 was co-precipitated with full-length α2-chimerin and the α1- and α2-common carboxy (C) terminus, but not with the α2-specific amino (N)-terminus (Figure 5B). These results show that EphA4 associates with α1-chimerin and α2-chimerin at their C termini.

Next we examined whether α-chimerin interacts with EphA4 in neurons, and, if so, whether ligand stimulation enhances the interaction. EphA4 was coprecipitated with α2-chimerin without ligand stimulation, and the amount of EphA4 precipitated with α2-chimerin was not increased following stimulation with clustered ephrinB3 (Figure 5C). These results indicate that α-chimerin associates with EphA4 in neurons and that this interaction is independent of ephrinB3-stimulation. Finally, we prepared lysates from the developing motor cortex of WT mice and immunoprecipitated them with anti-α2-chimerin antibody. EphA4 was again precipitated with α2-chimerin (Figure 5D).

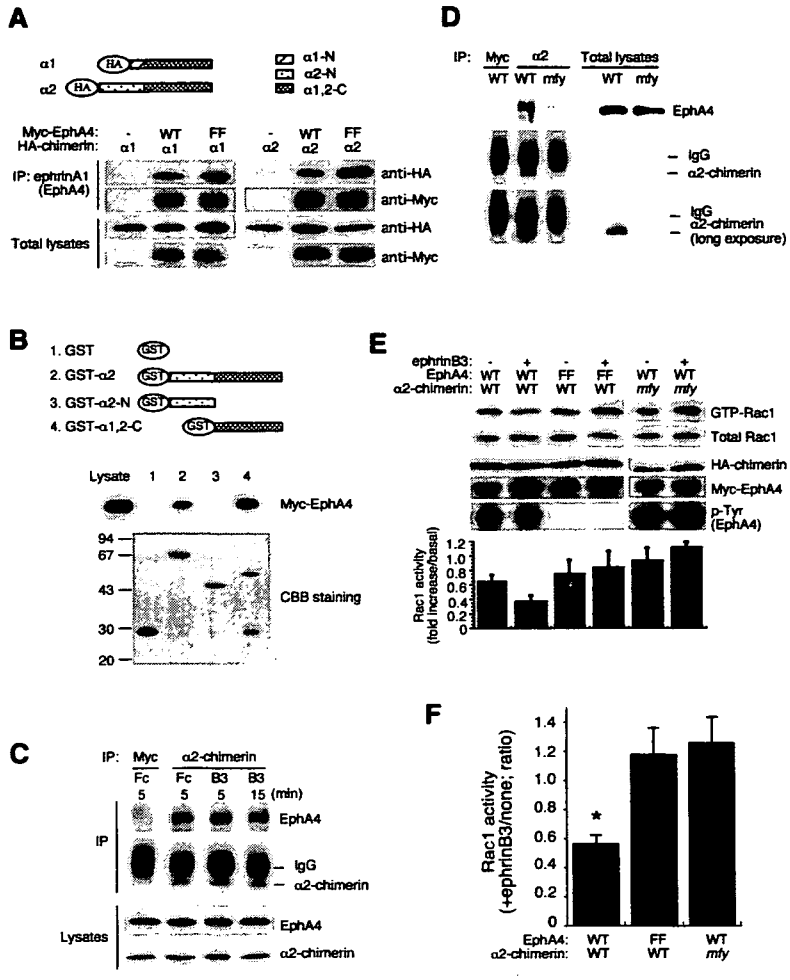


**Figure 5. α-Chimerin Interacts with EphA4 and Regulates Rac1 Activity in Response to EphrinB3 → EphA4 Forward Signaling**

(A) EphA4 bound to α1-chimerin and α2-chimerin in vitro. Kinase-dead EphA4$^{FF}$ also bound to both isoforms. 293T cells were transfected with the indicated expression plasmids. Total lysates were precipitated with Fc region-fused ephrinA1 and immunoblotted with anti-HA and anti-Myc antibodies to detect α-chimerin and EphA4, respectively. Total lysates were also blotted with anti-HA and anti-Myc antibodies.

(B) EphA4 interacted with the α-chimerin C terminus that is common to both α1 and α2 isoforms. For pulldown assays, HEK293T cells transfected with Myc-tagged EphA4 were lysed, and supernatants were incubated with GST-fusion proteins of α2-chimerin and its deletion mutants, followed by incubation with glutathione-Sepharose beads. Bound proteins were analyzed by SDS-PAGE and immunoblotting with anti-Myc antibody. The lower panel shows Coomassie brilliant blue (CBB) staining of GST-fusion proteins used in this experiment.

(C) Endogenous α-chimerin and EphA4 interacted in neurons, and ephrinB3-stimulation did not enhance this interaction. Cultured cortical neurons from E18.5 rats were stimulated with preclustered ephrinB3-Fc or control Fc for 5 or 15 min. Bound and total proteins were analyzed by immunoblotting with antibodies against EphA4 and α2-chimerin.

(D) Endogenous α-chimerin and EphA4 interacted in the mouse brain. Lysates from a P3 mouse cortex were immunoprecipitated with anti-α2-chimerin antibody or anti-Myc antibody (a negative control). The *mfy/mfy* cortex was used as a second negative control. Bound and total proteins were analyzed by immunoblotting with antibodies against EphA4 and α2-chimerin.

(E) COS-7 cells transfected with the indicated plasmids were stimulated with preclustered ephrinB3-Fc (+) or Fc (−) for 10 min. GTP-bound Rac1 was identified by SDS-PAGE and immunoblotting, and its levels were measured and normalized to the corresponding total Rac1 levels. The means and SEMs of Rac1 activity (fold increase/basal) are shown at the bottom.

(F) Statistical analysis of the data shown in (E). EphrinB3-stimulation inactivated Rac1 in cells expressing both EphA4$^{WT}$ and α-chimerin$^{WT}$, but not in cells expressing EphA4$^{FF}$ and α-chimerin$^{WT}$ or EphA4$^{WT}$ and α-chimerin$^{mfy}$. n = 4 (EphA4$^{WT}$ + α2-chimerin$^{WT}$), 5 (EphA4$^{FF}$ + α2-chimerin$^{WT}$), or 3 (EphA4$^{WT}$ + α2-chimerin$^{mfy}$). All data are presented as the mean ± SEM. (*$p < 0.05$, ANOVA/Tukey HSD).

## α-Chimerin Inactivates Rac in Response to EphrinB3/EphA4 Forward Signaling In Vitro

No previous reports have suggested the involvement of α-chimerin in ephrin/Eph signaling. To determine whether α-chimerin regulates Rac activity in response to ephrinB3/EphA4 forward signaling, we transfected COS-7 cells with EphA4 (EphA4$^{WT}$ or kinase-dead EphA4$^{FF}$) and α2-chimerin (α-chimerin$^{WT}$ or α-chimerin$^{mfy}$) and measured the Rac activity in the presence or absence of ephrinB3 stimulation (Figure 5E). We found that ephrinB3 stimulation inactivated Rac in cells expressing EphA4$^{WT}$ and α-chimerin$^{WT}$, but not in cells expressing either EphA4$^{FF}$ and α-chimerin$^{WT}$ or EphA4$^{WT}$ and α-chimerin$^{mfy}$ (Figure 5F). These results indicate that both EphA4 kinase activity and functional α-chimerin are required for ephrinB3 stimulation to inactivate Rac. It is noteworthy that the EphA4 proteins overexpressed in COS cells were phosphorylated, and, therefore, kinase active, but were unable to fully activate α-chimerin in the absence of ephrinB3 stimulation (Figure 5E). These results suggest that EphA4 kinase activity alone is not sufficient for activating the Rac-GAP of α-chimerin (see Discussion).

## Downregulation of α-Chimerin Suppresses EphrinB3-Induced Growth Cone Collapse in Cultured Cortical Neurons

EphrinB3/EphA4 forward signaling induces growth cone collapse in cultured neurons derived from the motor cortex (Egea et al., 2005; Kullander et al., 2001a). To determine whether α-chimerin regulates growth cone dynamics downstream of ephrinB3/EphA4 forward signaling, we performed two experiments. First, we cultured neurons

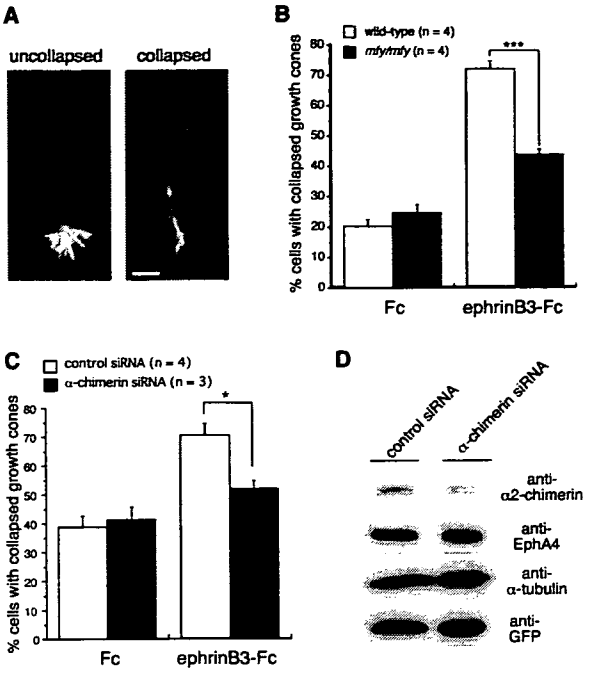


**Figure 6. Downregulation of α-Chimerin Suppresses EphrinB3-Induced Growth Cone Collapse**

(A) Representative examples of growth cones in phalloidin-stained cultured cortical neurons treated with preclustered Fc control (uncollapsed) or ephrinB3-Fc (collapsed). Scale bar: 10 μm.

(B) Growth cone collapse was induced by ephrinB3 in cultured neurons derived from the WT motor cortex, but was barely seen in those derived from the *mfy/mfy* cortex. All data are presented as the mean ± SEM of four independent experiments in each of which 100 neurons were counted (***$p < 0.001$, Student's t test).

(C) Downregulation of α-chimerin by siRNA suppressed ephrinB3-induced growth cone collapse in cultured cortical neurons. Cultured neurons derived from E18.5 rat cortex were transfected with a plasmid expressing both siRNA and enhanced yellow fluorescent protein (EYFP). In each experiment, 34–67 neurons expressing EYFP were counted. (*$p < 0.05$, Student's t test).

(D) α-chimerin-specific siRNA reduced the level of α-chimerin protein but not EphA4 protein. A 58.5% reduction of α-chimerin protein was observed in total lysates from cultured neurons in which 62% (not shown) of cells expressed α-chimerin-specific siRNA/EYFP, suggesting a drastic (>90%) reduction of α-chimerin.

derived from the motor cortex of WT and *mfy/mfy* mice on embryonic day 16.5 (E16.5) and then stimulated them with preclustered Fc or ephrinB3-Fc. EphrinB3 efficiently induced growth cone collapse in WT cortical neurons, as previously reported (Kullander et al., 2001a; Figures 6A and 6B); however, in the *mfy/mfy* cortical neurons, the frequency of collapse was significantly reduced (Figure 6B). Second, we expressed α-chimerin-specific siRNA by transfecting an expression vector into cultured neurons derived from the E18.5 rat motor cortex (Figure S8). The frequency of ephrinB3-induced growth cone collapse was significantly reduced in transected neurons (Figure 6C), and western blotting with the anti-α2-chimerin antibody demonstrated that α-chimerin protein levels were drastically reduced (>90%) in the transfected neurons (Figure 6D). We concluded that α-chimerin Rac-GAP acts downstream of ephrinB3/Eph signaling to cause growth cone collapse of cortical neurons.

Taken together, the results of our in vivo and in vitro studies confirm that α-chimerin Rac-GAP is a key molecule linking ephrinB3-induced EphA4 activation to the inactivation of Rac—a positive regulator of process outgrowth—thereby causing growth cone retraction and, eventually, axonal repulsion at the spinal cord midline.

## DISCUSSION

### α-Chimerin Is a Key Mediator of EphrinB3/EphA4 Forward Signaling and Causes Repulsion of CST Axons at the Spinal Cord Midline

We have shown the following. First, α-chimerin is colocalized with EphA4 in the developing CST (Figure S7). Second, it interacts with EphA4 both in vitro and in vivo (Figures 5A–5D). Third, when EphA4 is stimulated by ephrinB3, α-chimerin inactivates Rac, which is a positive regulator of process outgrowth, in vitro (Figure 5F). Fourth, ephrinB3-induced growth cone collapse is suppressed in cultured cortical neurons in which α-chimerin is downregulated by RNAi or *mfy* mutation (Figure 6). Fifth and finally, repulsion of CST axons at the spinal cord midline (Figures 1B and 4F) and formation of spinal CPGs (Figures 2C and 4G) are impaired in *mfy/mfy* mice and *α-Chn* KO mice, and both of these processes depend on ephrinB3/EphA4 forward signaling (Kullander et al., 2003, 2001a, 2001b; Yokoyama et al., 2001). Our results show that the Rac-GAP α-chimerin regulates CST axon guidance and CPG formation by mediating ephrinB3/EphA4 forward signaling (Figure 7).

It has been proposed that EphA receptors regulate growth cone dynamics through Rho-GEF ephexin1 (Shamah et al., 2001). During this process, activation of RhoA induces growth cone retraction and/or collapse, while activated Rac and Cdc42 promote its extension (Etienne-Manneville and Hall, 2002; Luo, 2000). The engagement of Ephs by ephrin leads to preferential activation of the exchange activity of ephexin toward RhoA, thus leading to growth cone collapse in vitro (Figure 7A; Shamah et al., 2001). We showed that the ephrin/Eph interaction leads to growth cone collapse due to Rac inactivation via the GAP activity of α-chimerin (Figure 7A). As both ephexin1 and α-chimerin are enriched in the central nervous system (Hall et al., 2001, 1993; Shamah et al., 2001), it is likely that the cooperative action of ephexin1-induced RhoA activation and α-chimerin-induced Rac inactivation function to induce retraction of growth cones during axon guidance in various circuits. *Ephexin1* KO mice appear to be normal (Sahin et al., 2005). This absence of an obvious phenotype might be due to compensation by other ephexin family members. Alternatively, it might be due to the activity of α-chimerin, which could prevent growth cone extension by inactivating Rac in response to ephrin/Eph signaling, even in the absence of

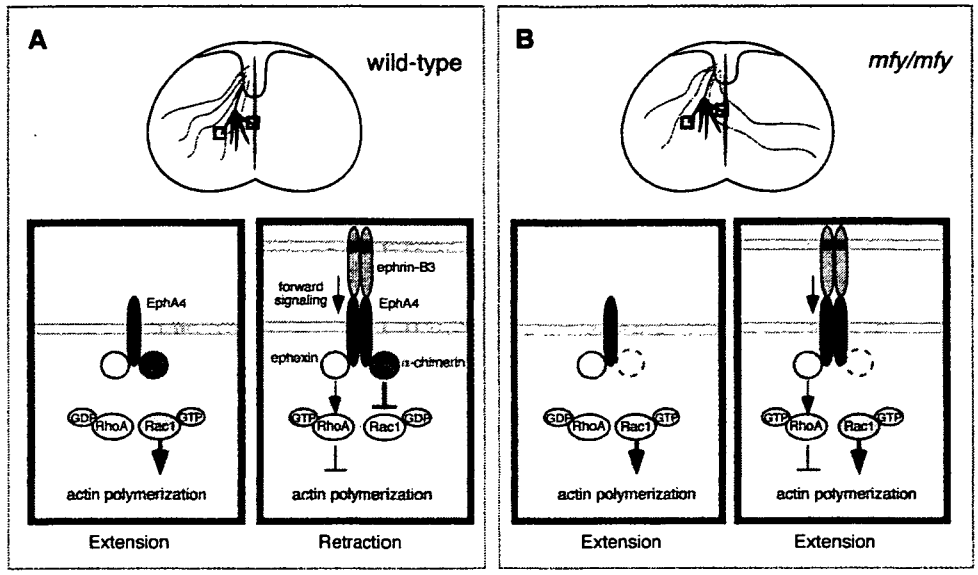


**Figure 7. Model of EphrinB3/EphA4 Forward Signaling in Midline Repulsion of CST Axons**

(A) In WT mice, the growth cones of CST axons extend due to basal activity of Rac, which is a positive regulator of process outgrowth, in the absence of ephrinB3 stimulation (green box). At the spinal cord midline that anchors ephrinB3, CST axons that express EphA4 receive forward signals. This ephrinB3/EphA4 forward signaling inactivates Rac through α-chimerin, leading to growth cone retraction (red box). Ephrin/EphA signaling might also activate RhoA, which is a negative regulator of process outgrowth, via ephexin (Shamah et al., 2001). The cooperative action of the RhoA-activator ephexin and the Rac-inactivator α-chimerin might induce efficient retraction of growth cones.

(B) In *mfy/mfy* mice, CST axons fail to stop at the midline due to the absence of α-chimerin-induced Rac inactivation, even in the presence of ephexin.

ephexin-induced RhoA activation. In contrast to the absence of an *Ephexin1* KO phenotype, we demonstrated that the formation of CST and CPGs is impaired in *α-Chn* mutant mice.

### Critical Role of Rho-GTPase Inactivation in Ephrin/Eph Signaling

Ephrin/Eph signaling is important in a wide range of biological processes, including oocyte maturation, early morphogenesis, segmentation, guidance of migrating cells, synaptic plasticity, dendritic-spine formation, and axon guidance (Flanagan and Vanderhaeghen, 1998; Palmer and Klein, 2003; Pasquale, 2005). Recent studies of in vitro orientation suggest that in various biological phenomena, ephrin/Eph signaling regulates actin dynamics by activating Rho-GTPases, such as RhoA, Rac, and Cdc42, through Rho-GEFs (Cowan et al., 2005; Fu et al., 2007; Irie and Yamaguchi, 2002; Murai and Pasquale, 2005; Ogita et al., 2003; Penzes et al., 2003; Shamah et al., 2001; Tanaka et al., 2004). We suggest that a further mode of ephrin/Eph signaling exists, in which Ephs regulate actin dynamics by inactivating Rho-GTPases through Rho-GAPs.

Ephrin/Eph signaling might control actin dynamics by regulating the balance between negative regulators of actin polymerization (such as RhoA) and positive regulators (such as Rac and Cdc42; Sahin et al., 2005; Shamah et al., 2001). This theory only takes into account Rho-activation; however, we have now shown that Rho-inactivation is another important aspect of the ephrin/Eph regulation of actin dynamics. The activity of each Rho-GTPase might be controlled by the balance between its activation by Rho-GEFs and its inactivation by Rho-GAPs. In mammalian cells, there are many diverse Rho-GEFs and Rho-GAPs with different substrate specificities that are controlled by different mechanisms (Etienne-Manneville and Hall, 2002). Thus, it is possible that ephrin/Eph signaling in different processes employs specific Rho-GEFs and/or Rho-GAPs to achieve the appropriate balance of activity of each Rho-GTPase. In short, we propose that ephrin/Eph signaling regulates actin dynamics in two ways: first, by regulating the balance between the activities of different Rho-GTPases (such as RhoA and Rac or Cdc42), and second, by regulating the balance between activation and inactivation of each individual Rho-GTPase.

### Regulation and Roles of α-Chimerin in Neural Development and Function

The present study provides evidence for the involvement of α-chimerin in ephrinB3/EphA4 forward signaling. How does ephrinB3/EphA4 signaling activate α-chimerin? As the kinase-inactive $EphA4^{FF}$ mutant protein could not activate α-chimerin (Figure 5F), it appeared that the kinase activity of EphA4 was necessary for the activation of α-chimerin. However, EphA4 kinase activity alone did not appear to be sufficient as the EphA4 proteins overexpressed in COS cells were phosphorylated and, thus,

kinase active, but were unable to fully activate α-chimerin in the absence of ephrinB3 stimulation (Figures 5E and 5F). In fact, it has been shown that the kinase activity of EphA4 alone is not sufficient for ephrinB/EphA4 forward signaling in vivo: the *EphA4*$^{EE/EE}$ mouse, the kinase of which is constitutively activated, has a normal alternate gait, normal CST axon midline guidance, normal CPG midline guidance, and normal morphology of the spinal cord (Egea et al., 2005). Cultured cortical neurons derived from *EphA4*$^{EE/EE}$ mice undergo normal growth cone collapse in response to clustered ephrinB3. Based on these observations, it has been proposed that higher-order clustering of EphA4 by stimulation of ephrinB is an essential component of ephrinB/EphA4 forward signaling (Egea et al., 2005). Our results are consistent with this idea.

Both the α1 and α2 isoforms of α-chimerin have a single copy of the C1 domain, which is a cysteine-rich motif, and can be activated by the binding of phorbol esters or diacylglycerol (DAG) to the C1 domain (Hall et al., 1990, 1993). Recently, it was reported that cyclin-dependent kinase 5 (Cdk5) regulates EphA4-mediated dendritic-spine retraction (Fu et al., 2007). Cdk5 is known to interact with α2-chimerin (Qi et al., 2004), so it is possible that a protein complex formed by clustering of EphA4 recruits some additional molecules required for linking activated EphA4 to α-chimerin activation. Such additional factors could include Cdk5/p35 and DAG-producing enzymes, such as phospholipase Cγ. It should be noted that these (or equivalent) factors do not appear to be specific to neurons, but rather are ubiquitous, as the expression of EphA4 and α2 isoforms in COS cells was sufficient to inactivate Rac upon stimulation by clustered-ephrinB3 (Figures 5E and 5F).

The *α-Chn* gene is widely expressed in the central nervous system both during development and in adulthood (Hall et al., 2001, 1990, 1993), and α-chimerin is found not only in axons but also in neuronal dendrites (Hall et al., 2001). It would be interesting to test whether α-chimerin plays a role in dendrite development in the brain. Recent studies using overexpression and/or siRNA-induced knockdown of α1-chimerin in cultured hippocampal neurons and cerebellar slices suggest that it regulates dendritic morphology and dendritic-spine density (Buttery et al., 2006; Van de Ven et al., 2005). α-chimerin might also be involved in NMDA receptor-dependent developmental plasticity, such as maturation of the barrel cortex (Iwasato et al., 2000, 1997), as well as in learning and memory, as it has been shown to interact with NMDA receptors in vitro (Van de Ven et al., 2005). The *mfy/mfy* mouse is thus a promising experimental model for elucidating the roles of α-chimerin Rac-GAP in the development and function of the central nervous system.

## EXPERIMENTAL PROCEDURES

### Animals

A Tg construct was made by modifying the RP23-413N9 BAC clone derived from B6 mouse genomic DNA (Roswell Park Cancer Institute, NY, USA). The Tg founder mice were generated by microinjection of linearized constructs into fertilized eggs. *α-Chn* KO mice were generated using MS12 ES cells derived from the B6 strain (for details see the Supplemental Experimental Procedures). All of the mice were maintained according to the institutional guidelines of the animal facilities of the RIKEN-BSI.

### VR Recordings

P1–P3 mice were anesthetized with isoflurane, and their spinal cords were removed as described elsewhere (Nishimaru et al., 2006). Electrical recordings of the VRs were made with glass-suction electrodes, and locomotor-like rhythmic activity was evoked by the concomitant bath application of NMDA (4–7 μM) and serotonin (5HT; 4–7 μM). Details of the recording procedure and data analyses are provided in the Supplemental Data.

### Linkage Analyses

PCR primers for the microsatellite markers and SNPs were designed using the Mouse Genome Informatics (http://www.informatics.jax.org/) and National Centre for Biotechnology Information (http://www.ncbi.nlm.nih.gov/SNP/) databases, respectively, and were verified by PCR using the genomic DNAs of inbred B6 and DBA/2 mice and B6/DBA $F_1$ hybrids (for detailed methods, see Figure S3 and Supplemental Data).

### Generation of Antibody

KLH-coupled synthetic peptides (MALTLFDTDEYRPPVWKC) corresponding to the N terminus of α2-chimerin (Figure S4A) were used to raise a rabbit polyclonal antibody (BSI Research Resources Center). Sera were affinity purified on the same peptides.

### Measurement of Rac1 Activity

Transfected COS-7 cells were stimulated with 2 μg/ml preclustered ephrinB3-Fc (R&D Systems) in serum-free medium for 10 min. The cells were lysed with ice-cold cell lysis buffer containing 4 μg of GST-CRIB of αPak (amino acids 70–150). After centrifugation, the supernatant was incubated with glutathione-Sepharose beads, and bound proteins were analyzed by SDS–PAGE and immunoblotting (for detailed methods, see Supplemental Data).

### Growth Cone Collapse Assay

Primary neurons were dissociated from the anterior dorsomedial to dorsal neocortex of E16.5 mice or E18.5 rats as described elsewhere (Ishikawa et al., 2003, Kullander et al., 2001a). The neurons were plated onto poly-D-lysine and laminin-coated coverslips and cultured in Neurobasal medium supplemented with 2% B27 (Invitrogen). They were then stimulated with 5 μg/ml preclustered ephrinB3-Fc for 30 min, fixed with 4% paraformaldehyde, and stained with rhodamine-conjugated phalloidin (Invitrogen; for detailed methods, see Supplemental Data).

### Supplemental Data

Supplemental Data include Experimental Procedures, References, nine figures, and one table and can be found with this article online at http://www.cell.com/cgi/content/full/130/4/742/DC1/.

## ACKNOWLEDGMENTS

We thank N. Ichinohe, S. Nishimura, Y. Sano, M. Tanaka, J. S. Park, and M. Fujita for advice on the experiments; T. Koganezawa for help with the analysis of electrophysiological data; T. Usami and H. Suzuki for technical assistance; H. Nishiyama for comments on the manuscript; the BSI Research Resources Center for animal care and technical assistance; J. Miyazaki and T. Saito for the CAG-EYFP vector; and K. Yaguchi for the pCR-FRT-amp-FRT plasmid. This work was supported, in part, by PRESTO, JST (to T.I.) and by a Grant-in-Aid for

Scientific Research on Priority Areas from the MEXT, Japan (to T.I. and H.K.).

Received: February 20, 2007
Revised: May 24, 2007
Accepted: July 16, 2007
Published: August 23, 2007

## REFERENCES

Ahmed, S., Lee, J., Wen, L.P., Zhao, Z., Ho, J., Best, A., Kozma, R., and Lim, L. (1994). Breakpoint cluster region gene product-related domain of n-chimaerin. Discrimination between Rac-binding and GTPase-activating residues by mutational analysis. J. Biol. Chem. *269*, 17642–17648.

Brown, M., Jacobs, T., Eickholt, B., Ferrari, G., Teo, M., Monfries, C., Qi, R.Z., Leung, T., Lim, L., and Hall, C. (2004). Alpha2-chimaerin, cyclin-dependent kinase 5/p35, and its target collapsin response mediator protein-2 are essential components in semaphorin 3A-induced growth-cone collapse. J. Neurosci. *24*, 8994–9004.

Buttery, P., Beg, A.A., Chih, B., Broder, A., Mason, C.A., and Scheiffele, P. (2006). The diacylglycerol-binding protein alpha1-chimaerin regulates dendritic morphology. Proc. Natl. Acad. Sci. USA *103*, 1924–1929.

Cowan, C.W., Shao, Y.R., Sahin, M., Shamah, S.M., Lin, M.Z., Greer, P.L., Gao, S., Griffith, E.C., Brugge, J.S., and Greenberg, M.E. (2005). Vav family GEFs link activated Ephs to endocytosis and axon guidance. Neuron *46*, 205–217.

Diekmann, D., Brill, S., Garrett, M.D., Totty, N., Hsuan, J., Monfries, C., Hall, C., Lim, L., and Hall, A. (1991). Bcr encodes a GTPase-activating protein for p21rac. Nature *351*, 400–402.

Dottori, M., Hartley, L., Galea, M., Paxinos, G., Polizzotto, M., Kilpatrick, T., Bartlett, P.F., Murphy, M., Kontgen, F., and Boyd, A.W. (1998). EphA4 (Sek1) receptor tyrosine kinase is required for the development of the corticospinal tract. Proc. Natl. Acad. Sci. USA *95*, 13248–13253.

Egea, J., Nissen, U.V., Dufour, A., Sahin, M., Greer, P., Kullander, K., Mrsic-Flogel, T.D., Greenberg, M.E., Kiehn, O., Vanderhaeghen, P., et al. (2005). Regulation of EphA 4 kinase activity is required for a subset of axon guidance decisions suggesting a key role for receptor clustering in Eph function. Neuron *47*, 515–528.

Eph Nomenclature Committee (1997). Unified nomenclature for Eph family receptors and their ligands, the ephrins. Cell *90*, 403–404.

Etienne-Manneville, S., and Hall, A. (2002). Rho GTPases in cell biology. Nature *420*, 629–635.

Flanagan, J.G., and Vanderhaeghen, P. (1998). The ephrins and Eph receptors in neural development. Annu. Rev. Neurosci. *21*, 309–345.

Fu, W.Y., Chen, Y., Sahin, M., Zhao, X.S., Shi, L., Bikoff, J.B., Lai, K.O., Yung, W.H., Fu, A.K., Greenberg, M.E., et al. (2007). Cdk5 regulates EphA4-mediated dendritic spine retraction through an ephexin1-dependent mechanism. Nat. Neurosci. *10*, 67–76.

Gianino, S., Stein, S.A., Li, H., Lu, X., Biesiada, E., Ulas, J., and Xu, X.M. (1999). Postnatal growth of corticospinal axons in the spinal cord of developing mice. Brain Res. Dev. Brain Res. *112*, 189–204.

Grillner, S., and Wallen, P. (1985). Central pattern generators for locomotion, with special reference to vertebrates. Annu. Rev. Neurosci. *8*, 233–261.

Hall, C., Monfries, C., Smith, P., Lim, H.H., Kozma, R., Ahmed, S., Vanniasingham, V., Leung, T., and Lim, L. (1990). Novel human brain cDNA encoding a 34,000 Mr protein n-chimaerin, related to both the regulatory domain of protein kinase C and BCR, the product of the breakpoint cluster region gene. J. Mol. Biol. *211*, 11–16.

Hall, C., Sin, W.C., Teo, M., Michael, G.J., Smith, P., Dong, J.M., Lim, H.H., Manser, E., Spurr, N.K., Jones, T.A., et al. (1993). Alpha 2-chimerin, an SH2-containing GTPase-activating protein for the ras-related protein p21rac derived by alternate splicing of the human n-chimerin gene, is selectively expressed in brain regions and testes. Mol. Cell. Biol. *13*, 4986–4998.

Hall, C., Michael, G.J., Cann, N., Ferrari, G., Teo, M., Jacobs, T., Monfries, C., and Lim, L. (2001). Alpha2-chimaerin, a Cdc42/Rac1 regulator, is selectively expressed in the rat embryonic nervous system and is involved in neuritogenesis in N1E–115 neuroblastoma cells. J. Neurosci. *21*, 5191–5202.

Inoue, H., Tsukita, K., Iwasato, T., Suzuki, Y., Tomioka, M., Tateno, M., Nagao, M., Kawata, A., Saido, T.C., Miura, M., et al. (2003). The crucial role of caspase-9 in the disease progression of a transgenic ALS mouse model. EMBO J. *22*, 6665–6674.

Irie, F., and Yamaguchi, Y. (2002). EphB receptors regulate dendritic spine development via intersectin, Cdc42 and N-WASP. Nat. Neurosci. *5*, 1117–1118.

Ishikawa, Y., Katoh, H., and Negishi, M. (2003). A role of Rnd1 GTPase in dendritic spine formation in hippocampal neurons. J. Neurosci. *23*, 11065–11072.

Iwasato, T., Erzurumlu, R.S., Huerta, P.T., Chen, D.F., Sasaoka, T., Ulupinar, E., and Tonegawa, S. (1997). NMDA receptor-dependent refinement of somatotopic maps. Neuron *19*, 1201–1210.

Iwasato, T., Datwani, A., Wolf, A.M., Nishiyama, H., Taguchi, Y., Tonegawa, S., Knopfel, T., Erzurumlu, R.S., and Itohara, S. (2000). Cortex-restricted disruption of NMDAR1 impairs neuronal patterns in the barrel cortex. Nature *406*, 726–731.

Kiehn, O., and Kullander, K. (2004). Central pattern generators deciphered by molecular genetics. Neuron *41*, 317–321.

Kullander, K., Croll, S.D., Zimmer, M., Pan, L., McClain, J., Hughes, V., Zabski, S., DeChiara, T.M., Klein, R., Yancopoulos, G.D., et al. (2001a). Ephrin-B3 is the midline barrier that prevents corticospinal tract axons from recrossing, allowing for unilateral motor control. Genes Dev. *15*, 877–888.

Kullander, K., Mather, N.K., Diella, F., Dottori, M., Boyd, A.W., and Klein, R. (2001b). Kinase-dependent and kinase-independent functions of EphA4 receptors in major axon tract formation *in vivo*. Neuron *29*, 73–84.

Kullander, K., Butt, S.J., Lebret, J.M., Lundfald, L., Restrepo, C.E., Rydstrom, A., Klein, R., and Kiehn, O. (2003). Role of EphA4 and EphrinB3 in local neuronal circuits that control walking. Science *299*, 1889–1892.

Liang, F.Y., Moret, V., Wiesendanger, M., and Rouiller, E.M. (1991). Corticomotoneuronal connections in the rat: evidence from double-labeling of motoneurons and corticospinal axon arborizations. J. Comp. Neurol. *311*, 356–366.

Luo, L. (2000). Rho GTPases in neuronal morphogenesis. Nat. Rev. Neurosci. *1*, 173–180.

Murai, K.K., and Pasquale, E.B. (2005). New exchanges in eph-dependent growth cone dynamics. Neuron *46*, 161–163.

Nishimaru, H., and Kudo, N. (2000). Formation of the central pattern generator for locomotion in the rat and mouse. Brain Res. Bull. *53*, 661–669.

Nishimaru, H., Restrepo, C.E., and Kiehn, O. (2006). Activity of Renshaw cells during locomotor-like rhythmic activity in the isolated spinal cord of neonatal mice. J. Neurosci. *26*, 5320–5328.

Noren, N.K., and Pasquale, E.B. (2004). Eph receptor-ephrin bidirectional signals that target Ras and Rho proteins. Cell. Signal. *16*, 655–666.

Ogita, H., Kunimoto, S., Kamioka, Y., Sawa, H., Masuda, M., and Mochizuki, N. (2003). EphA4-mediated Rho activation via Vsm-RhoGEF expressed specifically in vascular smooth muscle cells. Circ. Res. *93*, 23–31.

Palmer, A., and Klein, R. (2003). Multiple roles of ephrins in morphogenesis, neuronal networking, and brain function. Genes Dev. *17*, 1429–1450.

Pasquale, E.B. (2005). Eph receptor signalling casts a wide net on cell behaviour. Nat. Rev. Mol. Cell Biol. *6*, 462–475.

Penzes, P., Beeser, A., Chernoff, J., Schiller, M.R., Eipper, B.A., Mains, R.E., and Huganir, R.L. (2003). Rapid induction of dendritic spine morphogenesis by trans-synaptic ephrinB-EphB receptor activation of the Rho-GEF kalirin. Neuron *37*, 263–274.

Qi, R.Z., Ching, Y.P., Kung, H.F., and Wang, J.H. (2004). Alpha-chimerin exists in a functional complex with the Cdk5 kinase in brain. FEBS Lett. *561*, 177–180.

Sahin, M., Greer, P.L., Lin, M.Z., Poucher, H., Eberhart, J., Schmidt, S., Wright, T.M., Shamah, S.M., O'Connell, S., Cowan, C.W., et al. (2005). Eph-dependent tyrosine phosphorylation of ephexin1 modulates growth cone collapse. Neuron *46*, 191–204.

Shamah, S.M., Lin, M.Z., Goldberg, J.L., Estrach, S., Sahin, M., Hu, L., Bazalakova, M., Neve, R.L., Corfas, G., Debant, A., et al. (2001). EphA receptors regulate growth cone dynamics through the novel guanine nucleotide exchange factor ephexin. Cell *105*, 233–244.

Tanaka, M., Ohashi, R., Nakamura, R., Shinmura, K., Kamo, T., Sakai, R., and Sugimura, H. (2004). Tiam1 mediates neurite outgrowth induced by ephrin-B1 and EphA2. EMBO J. *23*, 1075–1088.

Van de Ven, T.J., VanDongen, H.M., and VanDongen, A.M. (2005). The nonkinase phorbol ester receptor alpha1-chimerin binds the NMDA receptor NR2A subunit and regulates dendritic spine density. J. Neurosci. *25*, 9488–9496.

Wahl, S., Barth, H., Ciossek, T., Aktories, K., and Mueller, B.K. (2000). Ephrin-A5 induces collapse of growth cones by activating Rho and Rho kinase. J. Cell Biol. *149*, 263–270.

Whelan, P., Bonnot, A., and O'Donovan, M.J. (2000). Properties of rhythmic activity generated by the isolated spinal cord of the neonatal mouse. J. Neurophysiol. *84*, 2821–2833.

Yokoyama, N., Romero, M.I., Cowan, C.A., Galvan, P., Helmbacher, F., Charnay, P., Parada, L.F., and Henkemeyer, M. (2001). Forward signaling mediated by ephrin-B3 prevents contralateral corticospinal axons from recrossing the spinal cord midline. Neuron *29*, 85–97.

**Accession Numbers**

The DNA sequences have been deposited in the DNA Data Bank of Japan (DDBJ) under the following accession numbers: AB264771 ($\alpha 1$-$Chn^{mfy}$ cDNA), AB264772 ($\alpha 2$-$Chn^{mfy}$ cDNA), AB264773 ($\alpha 3$-$Chn^{mfy}$ cDNA), AB264774 ($\alpha 3$-$Chn^{WT}$ cDNA), and AB264775 (retroposon).

ELSEVIER

Neurobiology of Disease

www.elsevier.com/locate/ynbdi
Neurobiology of Disease 23 (2006) 169 – 177

# Conditional knockout of Mn superoxide dismutase in postnatal motor neurons reveals resistance to mitochondrial generated superoxide radicals

Hidemi Misawa,[a,b,*] Kazuko Nakata,[a] Junko Matsuura,[a] Yasuhiro Moriwaki,[b] Koichiro Kawashima,[b] Takahiko Shimizu,[c] Takuji Shirasawa,[c] Ryosuke Takahashi[d,e]

[a]*Department of Neurology, Tokyo Metropolitan Institute for Neuroscience, 2-6, Musashidai, Fuchu-shi, Tokyo 183-8526, Japan*
[b]*Department of Pharmacology, Kyoritsu University of Pharmacy, 1-5-30, Shibakoen, Minato-ku, Tokyo 105-8512, Japan*
[c]*Department of Molecular Gerontology, Tokyo Metropolitan Institute of Gerontology, 35-2, Sakae-cho, Itabashi-ku, Tokyo 173-0015, Japan*
[d]*Laboratory for Motor System Neurodegeneration, RIKEN Brain Science Institute, 2-1, Hirosawa, Wako-shi, Saitama 351-0198, Japan*
[e]*Deparment of Neurology, Graduate School of Medicine, Kyoto University, 54, Sho-goin kawaramachi, Sakyo-ku, Kyoto 606-8507, Japan*

Received 22 November 2005; revised 24 January 2006; accepted 27 February 2006
Available online 3 May 2006

**Mitochondrial dysfunction and oxidative damage are implicated in the pathogenesis of neurodegenerative disease. Mice deficient in the mitochondrial form of superoxide dismutase (SOD2) die during embryonic or early postnatal development, precluding analysis of a pathological role for superoxide in adult tissue. Here, we generated postnatal motor neuron-specific SOD2 knockouts by crossing mice with floxed SOD2 alleles to VAChT-Cre transgenic mice in which Cre expression is restricted to postnatal somatomotor neurons. SOD2 immunoreactivity was specifically lost in a subset of somatomotor neurons resulting in enhanced superoxide production. Yet extensive histological examination revealed no signs of oxidative damage in animals up to 1 year after birth. However, disorganization of distal nerve axons following injury was accelerated in SOD2-deficient motor neurons. These data demonstrate that postnatal motor neurons are surprisingly resistant to oxidative damage from mitochondrial-derived superoxide radicals, but that such damage may sensitize axons to disorganization following nerve injury.**


*Keywords:* Motor neurons; Oxidative stress; Mitochondria; Nerve injury; Conditional knockout; SOD2; Amyotrophic lateral sclerosis

## Introduction

Oxygen radicals, of which superoxide ($O_2^{\bullet -}$) is the most abundant, are a natural byproduct of oxygen consumption by the respiratory chain in aerobic ATP production. The superoxide dismutases (SODs) are enzymes that catalyze the conversion of $O_2^{\bullet -}$ to hydrogen peroxide and thus help prevent the build up of toxic $O_2^{\bullet -}$ levels. Three SOD isoforms are expressed in mammalian cells: copper/zinc SOD (SOD1) located in the cytoplasm (McCord and Fridovich, 1969), manganese SOD (SOD2) located in the mitochondrial matrix (Weisiger and Fridovich, 1973) and extracellular SOD (SOD3) (Marklund, 1982; Hjalmarsson et al., 1987). A small fraction of SOD1 is also reported to reside in the intermembrane space of mitochondria (Okado-Matsumoto and Fridovich, 2001; Mattiazzi et al., 2002; Okado-Matsumoto and Fridovich, 2002).

Oxidative stress has been implicated in various neurodegenerative diseases including Parkinson's disease, Alzheimer's disease and amyotrophic lateral sclerosis (ALS). Though it remains unclear whether oxidative stress is a major cause or merely a consequence of cellular dysfunction associated with neurodegenerative diseases (Andersen, 2004), an accumulating body of evidence implicates impaired mitochondrial energy production and increased mitochondrial oxidative damage in early pathological events leading to neurodegeneration (Beal, 1996). Mitochondria are both a major source of reactive oxygen species (ROS) production as well as a major target of ROS-induced cellular injury. Thus, mitochondrial localized superoxide dismutase (SOD2) is thought to play an important role in cellular defense against oxidative damage by ROS.

Loss of SOD2 results in embryonic or early postnatal lethality that varies with genetic background. SOD2 knockout mice on a CD-1 background die either in utero or within 24 h after birth from severe dilated cardiomyopathy (Li et al., 1995). Similarly, C57BL/6 SOD2 knockout mice die at late embryonic or early neonatal stages from dilated cardiomyopathy (Huang et al., 2001; Ikegami et al., 2002). On a mixed C57BL/6 and 129/Sv background, SOD2 mutant mice survive for up to 18 days, develop a milder form of

* Corresponding author. Department of Pharmacology, Kyoritsu University of Pharmacy, 1-5-30, Shibakoen, Minato-ku, Tokyo 105-8512, Japan. Fax: +81 3 5400 2698.
*E-mail address:* misawa-hd@kyoritsu-ph.ac.jp (H. Misawa).
**Available online on ScienceDirect (www.sciencedirect.com).**

0969-9961/$ - see front matter © 2006 Elsevier Inc. All rights reserved.
doi:10.1016/j.nbd.2006.02.014

dilated cardiomyopathy and display a neurological phenotype (Lebovitz et al., 1996). In contrast, DBA/2J (D2) SOD2 mutant mice do not develop cardiomyopathy but instead develop severe metabolic acidosis and survive an average of 8 days (Huang et al., 2001). This phenotypic variation suggests that sensitivities to SOD2 deficiency are highly dependent on genetic modifiers that differ across strain and cell type.

Motor neurons are believed to be particularly susceptible to oxidative damage given the high metabolic requirement to sustain a large cell size and long axonal processes. Although motor neurons in cell culture are vulnerable to cell death mediated via calcium influx after exposure to glutamate, it is unclear how motor neurons respond to the overproduction of mitochondrial-derived ROS in vivo. To circumvent the early lethality of SOD2 knockout mice, we used a conditional gene deletion approach in which mice with floxed SOD2 genes (Ikegami et al., 2002) were mated with VAChT-Cre mice (Misawa et al., 2003) that express Cre recombinase in approximately 50% of postnatal somatic motor neurons. Here, we report that conditional loss of SOD2 in postnatal motor neurons results in elevated mitochondrial oxidative stress that fails to trigger signs of neurodegeneration under nonpathological conditions. In contrast, nerve axotomy revealed accelerated nerve disorganization, suggesting that adult motor neurons have relative resistance to mitochondrial-generated superoxide radicals unless stressed.

## Materials and methods

### *Mice*

C57BL/6 mice carrying the VAChT-Cre transgene (VAChT-Cre.Fast and VAChT-Cre.Slow) have been described previously (Misawa et al., 2003). C57BL/6 mice with floxed SOD2 alleles have been described elsewhere (Ikegami et al., 2002). Localization of the VAChT-Cre transgene in the VAChT-Cre.Slow mouse line to chromosome 4 was determined by FISH analysis (data not shown), and VAChT-Cre.Slow mice were used to direct motor neuron-specific Cre expression in this study. Homozygous floxed SOD2 mice (lox/lox) were crossed with VAChT-Cre.Slow heterozygote animals. The resulting double heterozygote animals ($SOD2^{lox/+}$; $Cre^{slow/-}$) were selected and mated with homozygote floxed SOD2 mice. All animals were genotyped for SOD2 allele (Ikegami et al., 2002) and the Cre transgene (Misawa et al., 2003) using tail DNA as described previously. Motor performance was analyzed using a rotarod treadmill (MK-600; Muromachi Kikai, Tokyo, Japan) at 28 rpm. Grip strength was measured using a Grip Strength Meter for Mouse (Model 57106; Stoelting, Wood Dale, IL). All animal protocols were approved by the Tokyo Metropolitan Institute for Neuroscience Institutional Animal Care and Use Committee.

### *Histological assessment and immunohistochemistry*

Mice were anesthetized with sodium pentobarbital and perfused through the aortic cone with phosphate-buffered saline (PBS), followed with 4% paraformaldehyde (PFA) in 0.1 M phosphate buffer (PB) at pH 7.4. Brains and spinal cords were removed and postfixed in the same fixative for 2 h and then immersed in 20% sucrose in PB overnight at 4°C. The tissue was sectioned at 20 μm on a freezing microtome. For paraffin-embedded section, tissues were transferred to 70% ethanol and embedded in paraffin as described (Ichikawa et al., 1997). Serial brain or spinal cord sections were cut at 5 μm. Sections were stained for Nissl substance with cresyl violet or Fluoro-Jade B (Chemicon) according to the manufacturer's protocol. For staining of SOD2, SOD1, ChAT, and CHT, paraffin-embedded sections were immunohistochemically processed as described elsewhere (Ichikawa et al., 1997) with diaminobenzidine (DAB) as a chromogen followed by poststaining with hematoxylin. Antibodies used are rabbit polyclonal anti-SOD2 antibody (1:2000; Stressgen Biotechnologies), rabbit polyclonal anti-SOD1 antibody (1:2000; Stressgen Biotechnologies), rabbit polyclonal anti-ChAT (1:10,000; Ichikawa et al., 1997), and rabbit polyclonal anti-CHT antibody (50 ng/ml; Misawa et al., 2001). To estimate frequencies of Cre-mediated recombination of the floxed SOD2 alleles, serial paraffin sections were stained with SOD2 and ChAT as above, and the number of positive cells was counted. More than 500 cells were analyzed in the spinal cord ventral horn and 200 cells in each of the brainstem motor nucleus (from at least 3 mice at respective age). Double labeling for SOD2 and SMI-32 was performed by immunofluorescence. Sections were incubated simultaneously with rabbit polyclonal anti-SOD2 antibody (1:500; Stressgen Biotechnologies) and mouse SMI-32 monoclonal antibody to neurofilaments (1:1,000; Sternberger Monoclonals). Texas red-conjugated goat anti-mouse IgG was used to detect SMI-32-positive cells, and fluorescein isothiocyanate-conjugated goat anti-rabbit IgG was used to detect SOD2-expressing cells (1:200; Jackson Immunoresearch Labs).

### *In situ detection of $O_2^{\bullet -}$ production*

The spatial production of $O_2^{\bullet -}$ was investigated by in situ detection of oxidized hydroethidine (HEt; Molecular Probes) as previously described (Murakami et al., 1998). HEt is oxidized to a red fluorescent dye (ethidium) in living cells selectively by $O_2^{\bullet -}$, but not by other reactive oxygen species such as hydrogen peroxide, hydroxyl radical, or peroxynitrite (Bindokas et al., 1996). Briefly, HEt solution (0.2 ml; stock solution of HEt, 100 mg/ml in DMSO, diluted to 1 mg/ml in PBS) was intravenously injected 30 min before the animals were sacrificed. The animals were perfused with 4% paraformaldehyde as described above. Brain and spinal cord sections (20 μm) were cut on a cryostat and processed for fluorescent microscopy.

### *Hypoglossal nerve axotomy*

Nine-month-old mice ($SOD2^{lox/lox}$;$Cre^{slow/-}$ or $SOD2^{lox/lox}$; $Cre^{-/-}$) were anesthetized with an intraperitoneal injection of ketamine (80 mg/kg) and xylazine (12 mg/kg). The right hypoglossal nerve was exposed under the digastric muscle and transected with scissors. After 5 weeks, the animals were reanesthetized and perfused with 4% paraformaldehyde. The brainstem was removed, 5-μm serial paraffin-embedded sections were prepared and stained with cresyl violet as described above. Hypoglossal motor neurons with distinct clear nuclei in every eighth section (total 8 sections per animal) were counted.

### *Analysis of Wallerian degeneration*

Two days after unilateral transection of hypoglossal nerves as described above, mice were sacrificed by over-dose of sodium pentobarbital, the swollen first 2 mm of the distal nerve was discarded, the next 2 mm was used for morphological analysis, and a segment 4–7 mm distal to the lesion site was used for Western blotting. For morphological analysis, the nerve segments were fixed

for 1 day in 2% paraformaldehyde, 2% glutaraldehyde in 50 mM phosphate buffer, pH 7.4 (PB). Samples were treated in 1% $OsO_4$ in PB, washed, dehydrated with ethanol and then propylene oxide, and finally embedded in Quetol 812 epoxy resin (Nisshin EM, Tokyo, Japan). Semithin cross-sections (0.5 μm) for light microscopy were stained with toluidine blue.

*Electron microscopy*

Animals were perfused with 2% glutaraldehyde, 2% paraformaldehyde, 5% sucrose in 50 mM phosphate buffer (pH 7.4). The brain and spinal cord were removed and postfixed in the same fixative for 1 d at 4°C. The facial nucleus and spinal cord ventral horn were cut into 1- to 2-mm square pieces, fixed in 1% osmium tetroxide for 1 h at 4°C, dehydrated through a graded series of ethanol solutions and into propylene oxide, and embedded in Quetol 812 (Nissin EM). Ultra-thin sections were stained with lead citrate and uranyl acetate and examined with an electron microscope (H7500; Hitachi, Tokyo, Japan) at 10,000× magnification.

*Analysis of muscle atrophy and denervation*

Fresh skeletal muscle biopsies were obtained and frozen by immersion in isopentane cooled in liquid nitrogen. Sections were

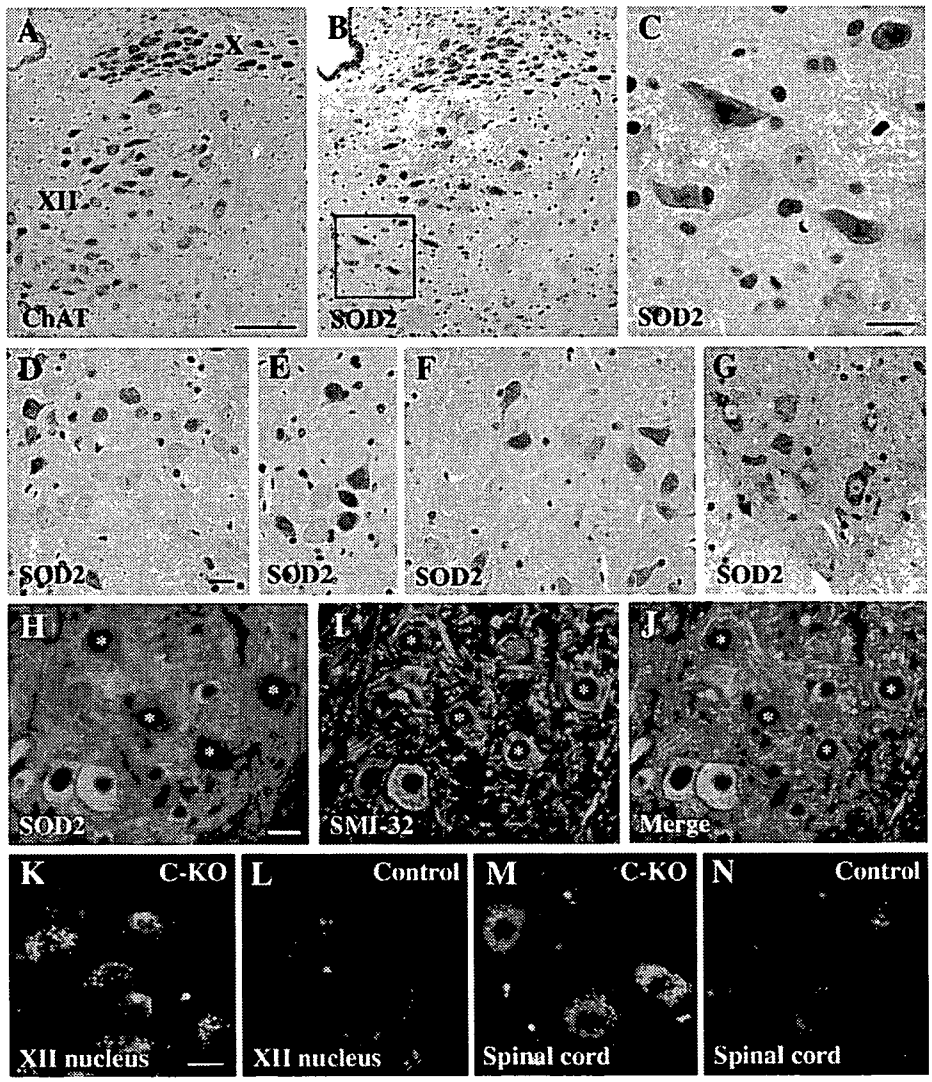


Fig. 1. Loss of SOD2 immunoreactivity in motor neurons from $SOD2^{lox/lox}$;$Cre^{slow/-}$ mice. (A–G) Paraffin-embedded sections of brain and spinal cord from $SOD2^{lox/lox}$;$Cre^{slow/-}$ mice at 5 months old stained with anti-ChAT antibody (A) or anti-SOD2 antibody (B-G). SOD2 immunoreactivity was lost in a subset of ChAT-positive somatomotor neurons as revealed by serial section through the hypoglossal nuclei (A–C) as well as sections through the oculomotor (D), abducens (E), facial (F) nuclei, and the ventral horn of the spinal cord (G). Note that SOD2 immunoreactivity was preserved in visceromotor neurons in the dorsal motor nucleus of the vagus (B). X, dorsal motor nucleus of the vagus; XII, hypoglossal nucleus. The boxed area in B is enlarged in panel C. (H–J) Paraffin-embedded sections from the ventral horn of the spinal cord were double-stained by immunofluorescence with anti-SOD2 (H) and anti-SMI-32 (I) antibodies. The merged image is shown in panel J. SOD2 immunoreactivity was lost in a subset of SMI-32-positive large motor neurons (denoted by asterisks) but not in SMI-32-negative small-diameter interneurons. (K–N) Mitochondrial production of $O_2^{\bullet -}$ was increased in $SOD2^{lox/lox}$;$Cre^{slow/-}$ (C-KO) mice compared with $SOD2^{lox/lox}$;$Cre^{-/-}$ (Control) mice in motor neurons in the hypoglossal nucleus (K and L) and ventral horn of the spinal cord (M and N) as revealed by HEt oxidation. HEt signals were detected in motor neurons as small granular particles in the cytosol, indicating mitochondrial production of $O_2^{\bullet -}$ under normal physiological conditions. Scale bars = 100 μm (A; also applies to B); 20 μm (C); 20 μm (D; also applies to E–G); 20 μm (H; also applies to I, J); 20 μm (K; also applies to L–N).

cut at 10 μm and processed for hematoxylin–eosin (H&E) or Gomori trichrome staining.

*Western blotting*

Cytoskeletal protein preservation was determined as described by Mack et al. (2001). Briefly, axotomized or control (uncut) hypoglossal nerves (3-mm length) were homogenized in 50 μl 25 mM Tris–HCl (pH 7.5), 2% SDS, 1 mM EDTA, 1× Complete protease inhibitor cocktail (Roche). Proteins (20 μl each) were separated using a 5–20% gradient polyacrylamide-SDS gel and semi-dry transferred onto a nylon membrane (Immobilon-P; Millipore). Loading and transfer were checked by staining with Ponceau S (Sigma). The membranes were incubated with monoclonal N52 antibody (Sigma) against neurofilament heavy chain diluted at 1:3000 in 5% nonfat skim milk/0.1% Tween 20 in PBS, followed by incubation with horseradish peroxidase-conjugated anti-mouse IgG (Bio-Rad), and visualized with ECL Western Blotting Detection Reagent (Amersham Pharmacia Biosciences). The same blots were reprobed with monoclonal antibody β-tub 2.1 (1:10,000; Sigma) against β-tubulin. In order to compare SOD2 expression between $SOD2^{lox/lox}$;$Cre^{slow/-}$ and $SOD2^{lox/lox}$;$Cre^{-/-}$ mice, ventral halves of the cervical spinal cord (5-mm length) were micro-dissected, homogenized, and processed for immunoblot analysis as described above with rabbit polyclonal anti-SOD2 antibody (1:10,000; Stressgen Biotechnologies), rabbit polyclonal anti-SOD1 antibody (1:10,000; Stressgen Biotechnologies), and mouse monoclonal anti-actin antibody (1 μg/ml; Chemicon).

## Results

*Generation of motor neuron-specific SOD2 knockout mice*

To generate postnatal motor neuron-specific SOD2 knockout mice, we crossed mice homozygous for floxed SOD2 alleles (Ikegami et al., 2002) with VAChT-Cre.Slow mice in which Cre expression is restricted in postnatal somatomotor neurons (Misawa et al., 2003). The VAChT-Cre.Fast line was not used in this study because the transgene integrated on the same chromosome as SOD2 (chromosome 17). Double heterozygote animals ($SOD2^{lox/+}$;$Cre^{slow/-}$) were again mated with homozygous floxed SOD2 mice. $SOD2^{lox/lox}$;$Cre^{slow/-}$ mice were born at a Mendelian ratio and survived to adulthood with no gross defects (data not shown). Furthermore, no signs of motor deficits, including tremor and paralysis, or muscle weakness were observed for up to 12 months as revealed by a rotarod test and grip strength measurements, respectively. Motor neurons in $SOD2^{lox/lox}$;$Cre^{slow/-}$ mice showed normal cell morphology, including soma size, and normal immunoreactivity for cholinergic markers such as choline acetyltransferase (ChAT; Figs. 1A and 2A–F), vesicular acetylcholine transporter (VAChT) and high-affinity choline transporter (CHT). In the brain stem and spinal cord, approximately 50% of ChAT-positive motor neurons lost mitochondrial SOD2 immunoreactivity, suggesting successful targeting of the SOD2 gene (Figs. 1A–J). The SOD2-negative motor neurons were observed in various somatomotor nuclei of the brainstem and spinal cord, but not in visceromotor nuclei such as the dorsal motor nucleus of the vagus. Also double immunofluorescence for SOD2 and SMI-32 (a marker for motor

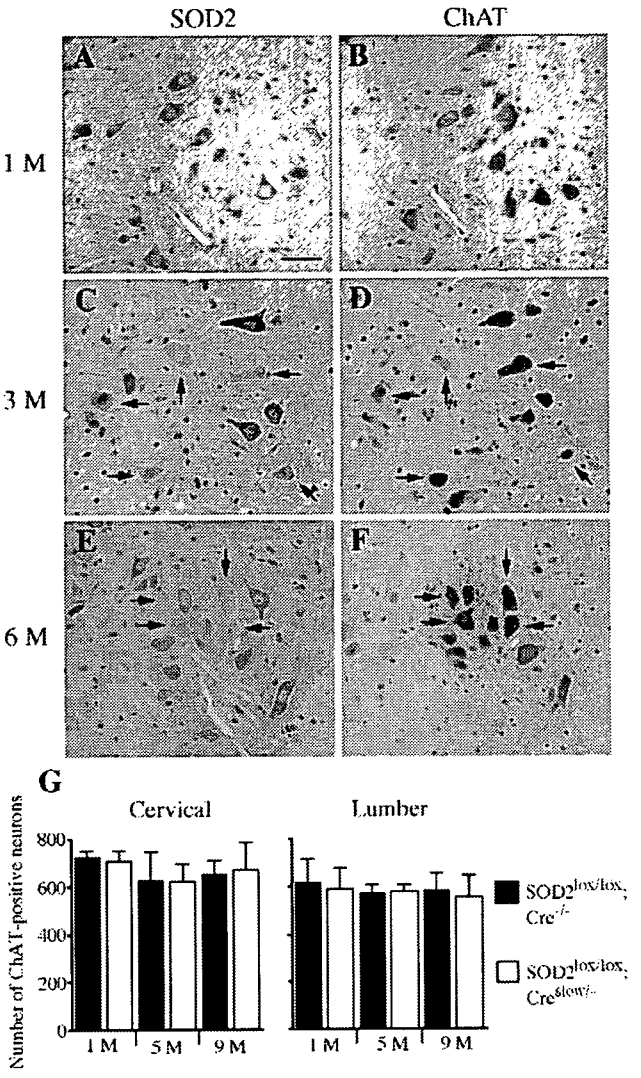


Fig. 2. Detection of SOD2-deficient and ChAT-positive motor neurons in the spinal cord of $SOD2^{lox/lox}$;$Cre^{slow/-}$ mice. Serial paraffin-embedded 5-μm sections of the lumber spinal cord from $SOD2^{lox/lox}$;$Cre^{slow/-}$ mice at 1 month (A, B), 3 months (C, D), or 6 months (E, F) of age were stained with anti-SOD2 (A, C, E) or anti-ChAT (B, D, F) antibodies. Arrows indicate SOD2-negative and ChAT-positive motor neurons. Scale bar = 50 μm. (G) Numbers of spinal cord ChAT-positive motor neurons in $SOD2^{lox/lox}$; $Cre^{slow/-}$ and $SOD2^{lox/lox}$;$Cre^{-/-}$ mice. Numbers were determined from every 5th section for a total of 15 sections. Shown are the means from three mice ± standard deviation ($n$ = 3).

neurons) reveals that SOD2 immunoreactivity was lost specifically in SMI-32-positive motor neurons and not in SMI-32-negative spinal interneurons (Figs. 1H–J).

*Increased production of $O_2^{\bullet -}$ by mitochondria in $SOD2^{lox/lox}$; $Cre^{slow/-}$ mice*

To examine the effect of loss of SOD2 on superoxide production, we compared the spatial production of $O_2^{\bullet -}$ between $SOD2^{lox/lox}$; $Cre^{slow/-}$ and $SOD2^{lox/lox}$; $Cre^{-/-}$ mice by using HEt, a $O_2^{\bullet -}$-specific fluorescent dye (Figs. 1K–N). In the brainstem and spinal cord, punctate ethidium signals in the cytosol reflecting mitochondrial production of $O_2^{\bullet -}$ were detected in motor neurons with large somas, suggesting a relatively high mitochondrial respiratory rate in these

cells under normal physiological conditions. The cytosolic punctate fluorescence of oxidized HEt was more intense in $SOD2^{lox/lox}$;$Cre^{slow/-}$ mice compared to $SOD2^{lox/lox}$;$Cre^{-/-}$ mice in a subset of hypoglossal and spinal cord motor neurons, confirming enhanced production of $O_2^{\bullet -}$ by mitochondria in $SOD2^{lox/lox}$;$Cre^{slow/-}$ mice. On the other hand, this increase in HEt fluorescence was not observed in visceral motor neurons such as the dorsal motor nucleus of the vagus in $SOD2^{lox/lox}$;$Cre^{slow/-}$ mice (data not shown).

### *Normal neurological and neurochemical profile of $SOD2^{lox/lox}$;$Cre^{slow/-}$ mice*

Despite the loss of SOD2 expression and increased superoxide production in motor neurons by 3 months of age (Figs. 2A–F), the number of ChAT-positive motor neurons in the cranial and lumber spinal cord was not significantly different between $SOD2^{lox/lox}$;$Cre^{slow/-}$ and $SOD2^{lox/lox}$;$Cre^{-/-}$ mice at either 5 or 9 months of age (Fig. 2G). Neither overt cell loss nor vacuolar changes in neurons or neuropil were observed as revealed by Nissl-staining of SOD2-negative motor neurons (Figs. 3A–D). Also analyzed was neuronal degeneration by Fluoro-Jade B (Schmued et al., 1997). No Fluoro-Jade B-positive neurons were detected in brain and spinal cord sections from either $SOD2^{lox/lox}$;$Cre^{slow/-}$ or $SOD2^{lox/lox}$; $Cre^{-/-}$ mice (not shown).

As free radicals are a potential source of damage to cellular constituents such as DNA, lipids, and proteins, we evaluated $SOD2^{lox/lox}$;$Cre^{slow/-}$ mice for histochemical signs of oxidative injury and stress. Yet SOD2-deficient motor neurons failed to react with any of the following antibodies: anti-SMI-31 monoclonal antibodies (Sternberger Monoclonals) to phosphorylated neurofilaments which are shown to be accumulated in nerve cell bodies under pathological conditions; a monoclonal antibody against 8-hydroxy-2-deoxyguanosine (8-OHdG; JAICA, Shizuoka, Japan) to oxidative DNA damage; a polyclonal anti-malondialdehyde antibody (MDA; Alpha Diagnostic International, San Antonio, TX) to lipid peroxidation-related MDA-protein adduct; or a monoclonal anti-nitrotyrosine antibody (Upstate Cell Signaling, Lake Placid, NY) to peroxynitrite-mediated protein modification.

A small fraction of SOD1 is reported to reside in the intermembranous space of mitochondria (Okado-Matsumoto and Fridovich, 2001; Mattiazzi et al., 2002; Okado-Matsumoto and Fridovich, 2002) where it may work as an additional line of defense against $O_2^{\bullet -}$. However, immunohistochemical staining showed no obvious compensatory overexpression of SOD1 in the SOD2-deficient motor neurons (Figs. 3E and F). It is still tempting to speculate that an increased amount of SOD1 is accumulated in mitochondria under the SOD2-deficient conditions. A detailed analysis of SOD2 subcellular localization using confocal microscopy or immunoelectron microscopy will be needed to address the possibility.

Next, we analyzed SOD2 expression in ventral halves of the cervical spinal cord micro-dissected from 9-month-old $SOD2^{lox/lox}$; $Cre^{slow/-}$ and $SOD2^{lox/lox}$;$Cre^{-/-}$ mice by immunoblot analysis (Fig. 3G). A significant decrease (30% by densitometry) in SOD2 content was evident in $SOD2^{lox/lox}$;$Cre^{slow/-}$ mice, although again SOD1 expression was unchanged. Even though SOD2 immunoreactivity is most strong in motor neurons in spinal cord sections, the homogenates include mitochondria from various other cell types such as glia and interneurons. Thus, the result shows that SOD2 expression was lost in 30% of the spinal motor neurons at the very least.

Finally, an ultrastructural analysis of mitochondria in motor neurons was undertaken using electron microscopy. Sections of the facial nucleus and spinal cord from 9-month-old $SOD2^{lox/lox}$; $Cre^{slow/-}$ and $SOD2^{lox/lox}$;$Cre^{-/-}$ mice were analyzed. Over 1000 mitochondria in each brain regions were examined, but no degenerative changes such as swelling, disorganization of the cristae or vacuolar formation were observed ($n$ = 3 for each genotype; data not shown).

As no obvious phenotype was detected in the cell bodies or organelles of SOD2-deficient motor neurons, we next analyzed the function of axonal processes by looking for muscle denervation and atrophy. Muscle biopsies from $SOD2^{lox/lox}$;$Cre^{slow/-}$ mice revealed

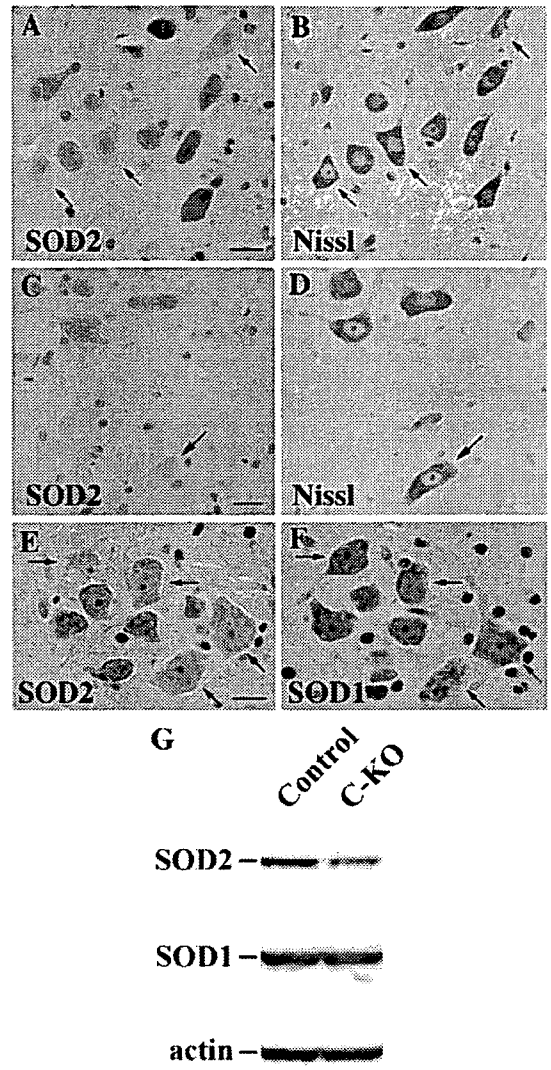


Fig. 3. Morphology of SOD2-deficient motor neurons in 9-month-old $SOD2^{lox/lox}$;$Cre^{slow/-}$ mice. Serial sections from the facial nucleus (A, B) or spinal cord ventral horn (C, D) stained with an anti-SOD2 antibody (A, C) or cresyl violet (Nissl; B, D). No overt morphological changes were seen in the SOD2-defiecent motor neurons (arrows). Serial sections from the hypoglossal nucleus stained with anti-SOD2 (E) or anti-SOD1 (F) antibodies. No difference in the staining pattern or intensity was evident between SOD2-negative (arrows) and SOD2-positive motor neurons. Scale bars = 20 μm. (G) Ventral portions of the spinal cord were micro-dissected from $SOD2^{lox/lox}$;$Cre^{slow/-}$ (C-KO) and $SOD2^{lox/lox}$;$Cre^{-/-}$ (Control) mice. Total homogenates (10 μg) were subjected to immunoblot analysis with polyclonal anti-SOD2 or anti-SOD1 antibodies. Actin content is shown as a loading control.

neither signs of muscle degeneration nor denervation/remodeling of motor axon terminals (Fig. 4). Furthermore, no evidence of reactive gliosis was revealed in $SOD2^{lox/lox}$;$Cre^{slow/-}$ mice by GFAP staining (data not shown), despite its presence in the brainstem motor nuclei of SOD2-null mice (Melov et al., 1998; Lynn et al., 2005).

*Motor neuron survival after hypoglossal nerve axotomy is unchanged*

Motor neurons in SOD1-deficient mice show an increased vulnerability to facial nerve axotomy despite an otherwise normal phenotype (Reaume et al., 1996). To test whether SOD2-deficient motor neurons are also more vulnerable to nerve injury, we employed unilateral transection of the hypoglossal nerve. Hypoglossal motor neuron survival was then assessed 5 weeks following transection (Fig. 5). Cell number in the axotomized hypoglossal nucleus decreased by approximately 10% compared to the contralateral control side, yet no statistical difference between $SOD2^{lox/lox}$;$Cre^{slow/-}$ and $SOD2^{lox/lox}$;$Cre^{-/-}$ mice was observed (Fig. 5). Furthermore, no difference in the number of SOD2-immunonegative cells was detected in $SOD2^{lox/lox}$;$Cre^{slow/-}$ mice after unilateral axotomy, and similar numbers of atrophic cells were seen in the transected nuclei of $SOD2^{lox/lox}$;$Cre^{slow/-}$ and $SOD2^{lox/lox}$;$Cre^{-/-}$ mice (data not shown).

*Motor nerve axon disorganization is accelerated after hypoglossal nerve axotomy*

Next, we analyzed the structural stability of the transected hypoglossal axon 2–4 mm distal to the lesion site 2 days postoperation. The distal segment of an injured nerve is known

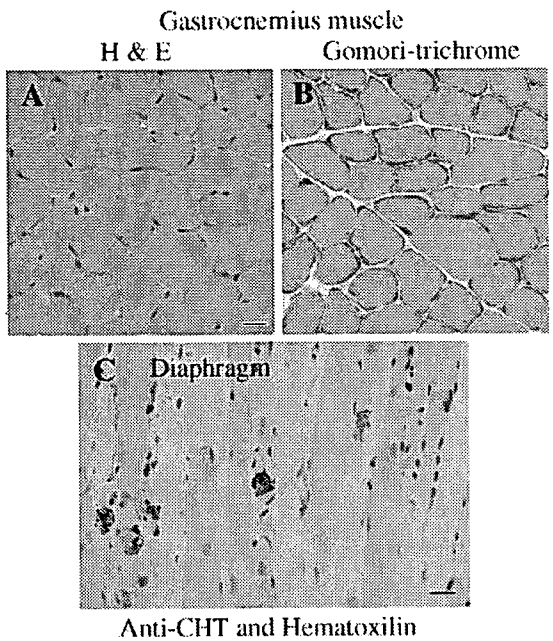


Fig. 4. Absence of muscle atrophy and denervation/remodeling of endplates in $SOD2^{lox/lox}$;$Cre^{slow/-}$ mice. Serial cryosections of gastrocnemius muscle from a 9-month-old $SOD2^{lox/lox}$;$Cre^{slow/-}$ mouse stained with hematoxylin and eosin (A) or Gomori-trichrome (B). Paraffin-embedded sections (5 μm) of diaphragm muscle containing neuromuscular junction from 9-month old $SOD2^{lox/lox}$;$Cre^{slow/-}$ mice stained with an anti-CHT antibody followed by counter-staining with hematoxylin (C). Scale bar = 20 μm.

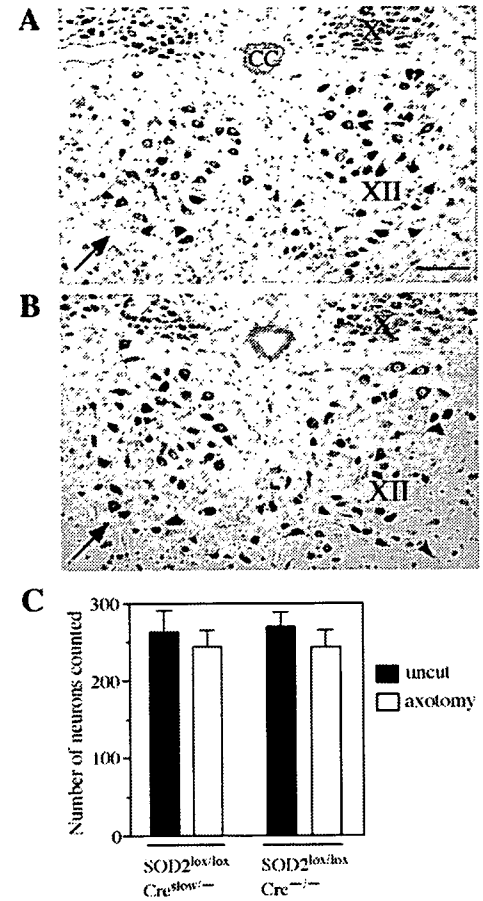


Fig. 5. Nissl-staining of hypoglossal motor neurons 5 weeks after axotomy in $SOD2^{lox/lox}$;$Cre^{slow/-}$ (A) and $SOD2^{lox/lox}$;$Cre^{-/-}$ (B) mice. Arrows indicate the operated side. CC, central canal; X, dorsal motor nucleus of the vagus; XII, hypoglossal nucleus. Scale bar = 100 μm. (C) Number of neurons in hypoglossal nuclei (uncut control or axotomized operated side) from both $SOD2^{lox/lox}$;$Cre^{slow/-}$ and $SOD2^{lox/lox}$;$Cre^{-/-}$ mice ($n$ = 4 for each genotype).

to undergo Wallerian degeneration within a few days. In the uncut contralateral nerve, we observed no difference in axon number and diameter between $SOD2^{lox/lox}$;$Cre^{slow/-}$ and $SOD2^{lox/lox}$;$Cre^{-/-}$ mice. However, $SOD2^{lox/lox}$;$Cre^{slow/-}$ axons did show an accelerated degeneration after nerve injury. When compared with $SOD2^{lox/lox}$;$Cre^{-/-}$ mice both cytoskeletal protein stability as revealed by Western blot and axon structure as revealed by histological analysis were significantly altered (Fig. 6).

## Discussion

The present study demonstrates for the first time that SOD2 is not required for postnatal motor neurons survival and further reveals that motor neurons are, in fact, quite resistant to mitochondrial generated $O_2^{\bullet -}$ in vivo. In the absence of SOD enzymatic activity, $O_2^{\bullet -}$ is relatively stable. Other antioxidants such as glutathione, ascorbate and tocopherols are relatively inefficient in removing superoxide radicals, and spontaneous dismutation occurs only very slowly. Because a portion of enzymatically active SOD1 is detected in the mitochondrial intermembranous space (Okado-Matsumoto and Fridovich, 2001; Mattiazzi

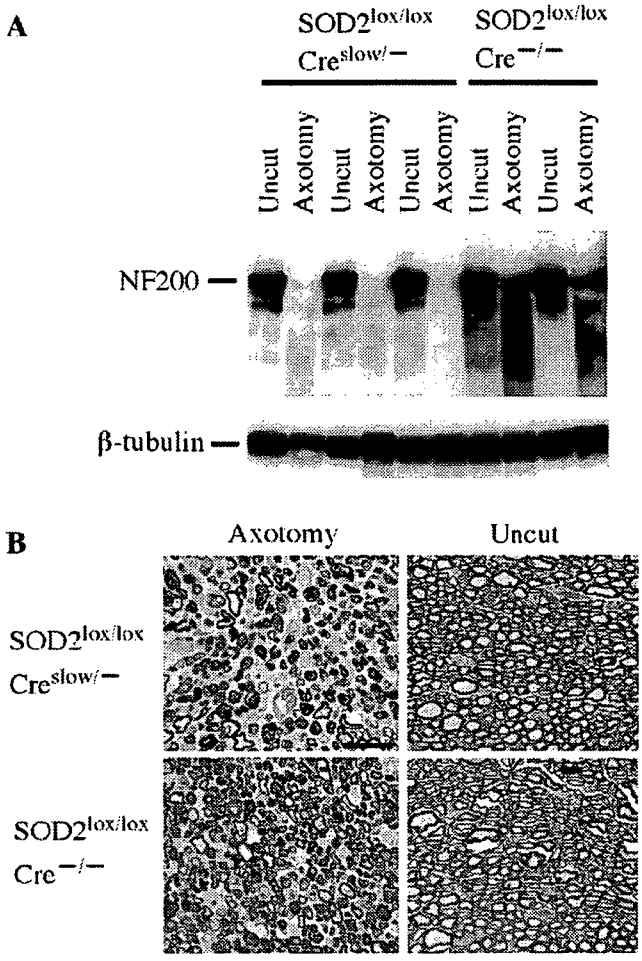


Fig. 6. Accelerated axonal disorganization in $SOD2^{lox/lox}$;$Cre^{slow/-}$ mice after motor nerve injury. (A) Western blot of 200-kDa neurofilament protein (NF-200) demonstrating the extent of degeneration 2 days after nerve transection in the distal transected hypoglossal nerve (Axotomy) or corresponding contralateral uncut nerve (Uncut). The blot was reprobed with control monoclonal antibody (β-tub 2.1) against β-tubulin. Samples from three $SOD2^{lox/lox}$;$Cre^{slow/-}$ and two $SOD2^{lox/lox}$;$Cre^{-/-}$ control mice are shown. (B) Representative toluidine blue-stained sections of hypoglossal nerves 2–4 mm distal to the lesion site 2 days after transection or corresponding contralateral uninjured nerve. Scale bar = 20 μm.

et al., 2002; Okado-Matsumoto and Fridovich, 2002), we speculate that, although the physiological functions of SOD1 in the mitochondria are not fully understood, some SOD2 function is compensated by SOD1 potentially by removing $O_2^{\bullet-}$ generated from complex III (Han et al., 2001). And although we did not detect SOD1 upregulation in SOD2-deficient motor neurons (Figs. 3E and F), endogenous levels of mitochondrial SOD1 may be sufficient to prevent both $O_2^{\bullet-}$-induced mitochondrial injury and $O_2^{\bullet-}$ release from mitochondria to cytosol. The physiological role and possible compensation of SOD2 loss by SOD1 can be addressed in future studies by crossing $SOD2^{lox/lox}$;$Cre^{slow/-}$ mice to a SOD1-null background.

Motor neurons in the SOD1-deficient mice are vulnerable to axotomy-induced oxidative burden (Reaume et al., 1996). In the present study, we have analyzed the effect of nerve transection on motor neurons lacking SOD2 expression. We demonstrate here that neuronal survival after axotomy is not affected, but that disorganization of distal nerve axons is accelerated in the SOD2-deficient motor neurons. Thus, loss of SOD2 function is insufficient to kill transected motor neurons but does trigger more rapid motor axon degeneration after nerve injury. Although we do not yet understand the mechanism underlying the observed accelerated disorganization, we speculate that abnormal $Ca^{2+}$ handling in SOD2-deficient mitochondria results in lowered $Ca^{2+}$-buffering activity specifically in lesioned distal axons while leaving the cell bodies unaffected. Interestingly, neurofilament proteins are known to be particularly susceptible tyrosine nitration and lysine oxidation (Beckman et al., 1993). Our present study thus implicates a previously unrecognized link between mitochondrial oxidative stress and axonal vulnerability to injury.

ALS is a fatal adult-onset neurodegenerative disease characterized by the selective loss of upper and lower motor neurons. Although its cause is not fully understood, mutations in the SOD1 gene cause a familial form of ALS, and recent studies show involvement of mitochondrial dysfunction and oxidative damage in ALS pathogenesis (Andersen, 2004; Bendotti and Carri, 2004; Bruijn et al., 2004; Xu et al., 2004). In animal models, mitochondrial abnormalities were seen in motor neurons of mice or rats expressing the SOD1 mutations $SOD1^{G93A}$ (Dal Canto and Gurney, 1994; Jaarsma et al., 2001; Howland et al., 2002) and $SOD1^{G37R}$ (Wong et al., 1995), but similar pathology was not detected in motor neurons expressing other types of mutant SOD1 (Bruijn et al., 1997; Nagai et al., 2001). Furthermore, Andreassen et al. (2000) reported that heterozygous loss of SOD2 exacerbates disease in mutant SOD1 transgenic mice. Recent studies show that mutant SOD1, rather than abrogating function, acquires a toxic function and that mutant SOD1 expression is required in both neurons and glia cells to induce motor neuron degeneration (Gong et al., 2000; Pramatarova et al., 2001; Lino et al., 2002; Clement et al., 2003). The present study also is consistent with a possible importance of interplay between neurons and glia cells in motor neuron survival.

In an ALS mouse model, expression of the neuronal isoform of nitric oxide synthase (nNOS) is increased in astrocytes surrounding motor neurons in the spinal cord and brainstem (Cha et al., 1998). Also increased nitrotyrosine labeling in motor neurons and in the ventral horn has been reported in ALS and mutant SOD1-expressing mouse models (Abe et al., 1995; Beal et al., 1997; Ferrante et al., 1997; Cha et al., 2000). In the present study, we did not find any nitrotyrosine immuno-positive cells in the brain and spinal cord of 9-month-old $SOD2^{lox/lox}$;$Cre^{slow/-}$ mice. Furthermore, neither signs of reactive gliosis (GFAP-IR) nor peroxynitrite-mediated oxidative damage (nitrotyrosine-IR) in astrocytes surrounding SOD2-deficient motor neurons were evident. We speculate that elevated levels of $O_2^{\bullet-}$ in motor neurons is not by itself enough to trigger chronic cell injury, but NO produced from neighboring astrocytes resulting in peroxynitrite production may be a further requirement to trigger ROS-induced toxicity.

Axonal disorganization and reduced slow axonal transport are well-known hallmarks of ALS. Although our present results indicate that loss of SOD2 function is not by itself sufficient to kill motor neurons in vivo, it does modify axonal susceptibility to nerve injury. Recently Vande Velde et al. (2004) reported that $Wld^S$ protein, the dominant neuroprotective factor that markedly delays Wallerian axonal degeneration after nerve injury, does not prevent SOD1-mediated motor neuron loss when introduced the $Wld^S$ mutation into the $SOD1^{G37R}$ or $SOD1^{G85R}$ ALS mouse models. These results show that inhibiting axonal degeneration is not

effective to ameliorate ALS pathogenesis induced by the mutant SOD1 protein.

Although the precise pathologic role of $O_2^{\bullet -}$ in motor neuron degeneration remains to be fully clarified, the present study is consistent with the possible involvement of nonneuronal cells in mitochondrial-derived, superoxide-induced injury in motor neurons. Thus, a rational therapeutic strategy that delivers antioxidants to surrounding astrocytes or microglia may significantly help motor neurons survive oxidative stress.

## Acknowledgments

The authors thank Drs. K. Amano and K. Yamakawa (RIKEN Brain Science Institute) for FISH analysis of VAChT-Cre.Slow mice; Drs. K. Endo and M. Ichikawa (Tokyo Metropolitan Institute for Neuroscience; TMIN) for valuable advice on electron microscopy; Drs. K. Kohyama, Y. Matsumoto, and T. Uchihara (TMIN) for muscle biopsy; and Dr. S. E. Craven for critical reading of the manuscript. This work was supported by grants from the Ministry of Education, Culture, Sports, Science and Technology, Japan, and from the Japanese Ministry of Health, Labor and Welfare, Research on Psychiatric and Neurological Diseases and Mental Health.

## References

Abe, K., Pan, L.-H., Watanabe, M., Kato, T., Itoyama, Y., 1995. Induction of nitrotyrosine-like immunoreactivity in the lower motor neuron of amyotrophic lateral sclerosis. Neurosci. Lett. 199, 152–154.

Andersen, J.K., 2004. Oxidative stress in neurodegeneration: cause or consequence? Nat. Med. 10, S18–S25 (Suppl.).

Andreassen, O.A., Ferrante, R.J., Klivenyi, P., Klein, A.M., Shinobu, L.A., Epstein, C.J., Beal, M.F., 2000. Partial deficiency of manganese superoxide dismutase exacerbates a transgenic mouse model of amyotrophic lateral sclerosis. Ann. Neurol. 47, 447–455.

Beal, M.F., 1996. Mitochondria, free radicals, and neurodegeneration. Curr. Opin. Neurobiol. 6, 661–666.

Beal, M.F., Ferrante, R.J., Browne, S.E., Matthews, R.T., Kowall, N.W., Brown Jr., R.H., 1997. Increased 3-nitrotyrosine in both sporadic and familial amyotrophic lateral sclerosis. Ann. Neurol. 42, 644–654.

Beckman, J.S., Carson, M., Smith, C.D., Koppenol, W.H., 1993. ALS, SOD and peroxynitrite. Nature 364, 584.

Bendotti, C., Carri, MT., 2004. Lessons from models of SOD1-linked familial ALS. Trends Mol. Med. 10, 393–400.

Bindokas, V.P., Jordan, J., Lee, C.C., Miller, R.J., 1996. Superoxide production in rat hippocampal neurons: selective imaging with hydroethidine. J. Neurosci. 16, 1324–1336.

Bruijn, L.I., Becher, M.W., Lee, M.K., Anderson, K.L., Jenkins, N.A., Copeland, N.G., Sisodia, S.S., Rothstein, J.D., Borchelt, D.R., Price, D.L., Cleveland, D.W., 1997. ALS-linked SOD1 mutant G85R mediates damage to astrocytes and promotes rapidly progressive disease with SOD1-containing inclusions. Neuron 18, 327–338.

Bruijn, L.I., Miller, T.M., Cleveland, D.W., 2004. Unraveling the mechanisms involved in motor neuron degeneration in ALS. Annu. Rev. Neurosci. 27, 723–749.

Cha, C.I., Kim, J.-M., Shin, D.H., Kim, Y.S., Kim, J., Gurney, M.E., Lee, K.W., 1998. Reactive astrocytes express nitric oxide synthase in the spinal cord of transgenic mice expressing a human Cu/Zn SOD mutation. NeuroReport 9, 1503–1506.

Cha, C.I., Chung, Y.H., Shin, C.-M., Shin, D.H., Kim, Y.S., Gurney, M.E., Lee, K.W., 2000. Immunocytochemical study on the distribution of nitrotyrosine in the brain of the transgenic mice expressing a human Cu/Zn SOD mutation. Brain Res. 853, 156–161.

Clement, A.M., Nguyen, M.D., Roberts, E.A., Garcia, M.L., Boillee, S., Rule, M., McMahon, A.P., Doucette, W., Siwek, D., Ferrante, R.J., Brown Jr., R.H., Julien, J.-P., Goldstein, L.S.B., Cleveland, D.W., 2003. Wild-type nonneuronal cells extend survival of SOD1 mutant motor neurons in ALS mice. Science 302, 113–117.

Dal Canto, MC., Gurney, M.E., 1994. Development of central nervous system pathology in a murine transgenic model of human amyotrophic lateral sclerosis. Am. J. Pathol. 145, 1271–1279.

Ferrante, R.J., Shinobu, L.A., Schulz, R.T., Matthews, R.T., Thomas, C.E., Kowall, N.W., Gurney, M.E., Beal, M.F., 1997. Increased 3-nitrotyrosine and oxidative damage in mice with a human copper/zinc superoxide dismutase mutation. Ann. Neurol. 42, 326–334.

Gong, Y.H., Parsadanian, A.S., Andreeva, A., Snider, W.D., Elliott, J.L., 2000. Restricted expression of G86R Cu/Zn superoxide dismutase in astrocytes results in astrocytosis but does not cause motoneuron degeneration. J. Neurosci. 20, 660–665.

Han, D., Williams, E., Cadenas, E., 2001. Mitochondrial respiratory chain-dependent generation of superoxide anion and its release into the intermembrane space. Biochem. J. 353, 411–416.

Hjalmarsson, K., Marklund, S.L., Engstrom, A., Edlund, T., 1987. Isolation and sequence of complementary DNA encoding human extracellular superoxide dismutase. Proc. Natl. Acad. Sci. U. S. A. 84, 6340–6344.

Howland, D.S., Liu, J., She, Y., Goad, B., Maragakis, N.J., Kim, B., Erickson, J., Kulik, J., DeVito, L., Psaltis, G., DeGennaro, L.J., Cleveland, D.W., Rothstein, J.D., 2002. Focal loss of the glutamate transporter EAAT2 in a transgenic rat model of SOD1 mutant-mediated amyotrophic lateral sclerosis (ALS). Proc. Natl. Acad. Sci. U. S. A. 99, 1604–1609.

Huang, T.T., Carlson, E.J., Kozy, H.M., Mantha, S., Goodman, S.I., Ursell, P.C., Epstein, C.J., 2001. Genetic modification of prenatal lethality and dilated cardiomyopathy in Mn superoxide dismutase mutant mice. Free Radical Biol. Med. 31, 1101–1110.

Ichikawa, T., Ajiki, K., Matsuura, J., Misawa, H., 1997. Localization of two cholinergic markers, choline acetyltransferase and vesicular acetylcholine transporter in the central nervous system of the rat: in situ hybridization histochemistry and immunohistochemistry. J. Chem. Neuroanat. 13, 23–39.

Ikegami, T., Suzuki, Y., Shimizu, T., Isono, K., Koseki, H., Shirasawa, T., 2002. Model mice for tissue-specific deletion of the manganese superoxide dismutase (MnSOD) gene. Biochem. Biophys. Res. Commun. 296, 729–736.

Jaarsma, D., Rognoni, F., van Duijn, W., Verspaget, H.W., Haasdijk, E.D., Holstege, J.C., 2001. CuZn superoxide dismutase (SOD1) accumulates in vacuolated mitochondria in transgenic mice expressing amyotrophic lateral sclerosis-linked SOD1 mutations. Acta Neuropathol. (Berlin) 102, 239–305.

Lebovitz, R.M., Zhang, H., Vogel, H., Cartwright Jr., J., Dionne, L., Lu, N., Huang, S., Matzuk, M.M., 1996. Neurodegeneration, myocardial injury, and perinatal death in mitochondrial superoxide dismutase-deficient mice. Proc. Natl. Acad. Sci. U. S. A. 93, 9782–9787.

Li, Y., Huang, T.-T., Carlson, E.J., Melov, S., Ursell, P.C., Olson, J.L., Noble, L.J., Yoshimura, M.P., Berger, C., Chan, P.H., Wallace, D.C., Epstein, C.J., 1995. Dilated cardiomyopathy and neonatal lethality in mutant mice lacking manganese superoxide dismutase. Nat. Genet. 11, 376–381.

Lino, M.M., Schneider, C., Caroni, P., 2002. Accumulation of SOD1 mutants in postnatal motoneurons does not cause motoneuron pathology or motoneuron disease. J. Neurosci. 22, 4825–4832.

Lynn, S., Huang, E.J., Elchuri, S., Naeemuddin, M., Nishinaka, Y., Yodoi, J., Ferriero, D., Epstein, M., Huang, C.J., 2005. Selective neuronal vulnerability and inadequate stress response in superoxide dismutase mutant mice. Free Radical Biol. Med. 38, 817–828.

Mack, T.G.A., Reiner, M., Beirowski, B., Mi, W., Emanuelli, M., Wagner, D., Thomson, D., Gillingwater, T., Court, F., Conforti, L., Fernando, F.S., Tarlton, A., Andressen, C., Addicks, K., Magni, G., Ribchester,

R.R., Perry, V.H., Coleman, M.P., 2001. Wallerian degeneration of injured axons and synapses is delayed by a Ube4b/Nmnat chimeric gene. Nat. Neurosci. 4, 1199–1206.

Marklund, S.L., 1982. Human copper-containing superoxide dismutase of high molecular weight. Proc. Natl. Acad. Sci. U. S. A. 79, 7634–7638.

Mattiazzi, M., D'Aurelio, M., Gajewski, C.D., Martushova, K., Kiaei, M., Beal, M.F., Manfredi, G., 2002. Mutated human SOD1 causes dysfunction of oxidative phosphorylation in mitochondria of transgenic mice. J. Biol. Chem. 277, 29626–29633.

McCord, J.M., Fridovich, I., 1969. The utility of superoxide dismutase in studying free radical reaction: I. Radicals generated by the interaction of sulfite, dimetyl sulfoxide, and oxygen. J. Biol. Chem. 244, 6056–6063.

Melov, S., Schneider, J.A., Day, B.J., Hinerfeld, D., Coskun, P., Mirra, S.S., Crapo, J.D., Wallace, D.C., 1998. A novel neurological phenotype in mice lacking mitochondrial manganese superoxide dismutase. Nat. Genet. 18, 159–163.

Misawa, H., Nakata, K., Matsuura, J., Nagao, M., Okuda, T., Haga, T., 2001. Distribution of the high-affinity choline transporter in the central nervous system of the rat. Neuroscience 105, 87–98.

Misawa, H., Nakata, K., Toda, K., Matsuura, J., Oda, Y., Inoue, H., Taneno, M., Takahashi, R., 2003. VAChT-Cre.Fast and VAChT-Cre.Slow: postnatal expression of Cre recombinase in somatomotor neurons with different onset. Genesis 37, 44–50.

Murakami, K., Kondo, T., Kawase, M., Li, Y., Sato, S., Chen, S.F., Chan, P.H., 1998. Mitochondrial susceptibility to oxidative stress exacerbates cerebral infarction that follows permanent focal cerebral ischemia in mutant mice with manganese superoxide dismutase deficiency. J. Neurosci. 18, 205–213.

Nagai, M., Aoki, M., Miyoshi, I., Kato, M., Pasinelli, P., Kasai, N., Brown Jr., R.H., Itoyama, Y., 2001. Rats expressing human cytosolic copper-zinc superoxide dismutase transgenes with amyotrophic lateral sclerosis: associated mutations develop motor neuron disease. J. Neurosci. 21, 9246–9254.

Okado-Matsumoto, A., Fridovich, I., 2001. Subcellular distribution of superoxide dismutases (SOD) in rat liver. J. Biol. Chem. 276, 38388–38393.

Okado-Matsumoto, A., Fridovich, I., 2002. Amyotrophic lateral sclerosis: a proposed mechanism. Proc. Natl. Acad. Sci. U. S. A. 99, 9010–9014.

Pramatarova, A., Laganiere, J., Roussel, J., Brisbois, K., Rouleau, G.A., 2001. Neuron-specific expression of mutant superoxide dismutase 1 in transgenic mice does not lead to motor impairment. J. Neurosci. 21, 3369–3374.

Reaume, A.G., Elliott, J.L., Hoffman, E.K., Kowall, N.W., Ferrante, R.J., Siwek, D.F., Wilcox, H.M., Flood, D.G., Beal, M.F., Brown Jr., R.H., Scott, R.W., Snider, W.D., 1996. Motor neurons in Cu/Zn superoxide dismutase-deficient mice develop normally but exhibit enhanced cell death after axonal injury. Nat. Genet. 13, 43–47.

Schmued, L.C., Albertson, C., Slikker Jr., W., 1997. Fluoro-Jade: a novel fluorochrome for the sensitive and reliable histochemical localization of neuronal degeneration. Brain Res. 751, 37–46.

Vande Velde, C., Garcia, M.L., Yin, X., Trapp, B.D., Cleveland, D.W., 2004. The neuroprotective factor $Wld^s$ does not attenuate mutant SOD1-mediated motor neuron disease. Neuromol. Med. 5, 193–203.

Weisiger, R.A., Fridovich, I., 1973. Mitochondrial superoxide dismutase: site of synthesis and intramitochondrial localization. J. Biol. Chem. 248, 4793–4796.

Wong, P.C., Pardo, C.A., Borchelt, D.R., Lee, M.K., Copeland, N.G., Jenkins, N.A., Sisodia, S.S., Cleveland, D.W., Price, D.L., 1995. An adverse property of a familial ALS-linked SOD1 mutation causes motor neuron disease characterized by vacuolar degeneration of mitochondria. Neuron 14, 1105–1116.

Xu, Z., Jung, C., Higgins, C., Levine, J., Kong, J., 2004. Mitochondrial degeneration in amyotrophic lateral sclerosis. J. Bioenerg. Biomembr. 36, 395–399.

nature neuroscience



# Chromogranin-mediated secretion of mutant superoxide dismutase proteins linked to amyotrophic lateral sclerosis

Makoto Urushitani[1], Attila Sik[2], Takashi Sakurai[3], Nobuyuki Nukina[3], Ryosuke Takahashi[4] & Jean-Pierre Julien[1]

**Here we report that chromogranins, components of neurosecretory vesicles, interact with mutant forms of superoxide dismutase (SOD1) that are linked to amyotrophic lateral sclerosis (ALS), but not with wild-type SOD1. This interaction was confirmed by yeast two-hybrid screen and by co-immunoprecipitation assays using either lysates from Neuro2a cells coexpressing chromogranins and SOD1 mutants or lysates from spinal cord of ALS mice. Confocal and immunoelectron microscopy revealed a partial colocalization of mutant SOD1 with chromogranins in spinal cord of ALS mice. Mutant SOD1 was also found in immuno-isolated trans-Golgi network and in microsome preparations, suggesting that it can be secreted. Indeed we report evidence that chromogranins may act as chaperone-like proteins to promote secretion of SOD1 mutants. From these results, and our finding that extracellular mutant SOD1 can trigger microgliosis and neuronal death, we propose a new ALS pathogenic model based on the toxicity of secreted SOD1 mutants.**

ALS is a progressive adult-onset neurodegenerative disorder that affects primarily motor neurons in the brain and spinal cord. The disease typically begins locally and spreads, leading to paralysis and death within 3–5 years. Approximately 10% of ALS cases are familial and 90% are sporadic. Mutations in the genes encoding SOD1 (ref. 1) are involved in 20% of familial ALS cases.

Despite a decade of investigation on familial ALS caused by missense mutations in the *SOD1* gene, the mechanism of toxicity to motor neurons has remained elusive. Transgenic mice expressing mutant forms of SOD1 develop motor neuron disease resembling ALS through a gain of unidentified deleterious properties[2]. Eliminating the copper chaperone for SOD1 does not diminish the toxicity of mutant SOD1 in mice[3], and mutations that disrupt the copper-binding site of mutant SOD1 do not suppress toxicity[4]. Thus, it is now thought that the toxicity of mutant SOD1 is not related to aberrant copper-mediated catalysis but rather to the propensity of the abnormal protein to aggregate, a phenomenon common to many neurodegenerative diseases[5,6]. Cell culture studies have shown that the mutant SOD1 proteins induce oxidative stress[7,8], form aggregates[9,10] and impair proteasomal function[11].

Notably, recent lines of evidence indicate that the toxicity of SOD1 mutants is non-cell-autonomous. The neuron-specific expression of mutant SOD1 does not provoke motor neuron disease[12,13]. Moreover, chimeric mouse studies with SOD1 mutants have demonstrated that neurodegeneration is delayed or eliminated when motor neurons expressing mutant SOD1 are surrounded by healthy wild-type cells[14]. Moreover, these studies show evidence of damage to wild-type motor neurons by surrounding cells expressing mutant SOD1. Such results emphasize the importance of a motor neuron milieu, but the mechanism by which the toxicity of mutant SOD1 may be transferred from one cell to another is still unclear[14].

So far, proteins known to interact with mutant forms of SOD1 but not with wild-type SOD1 have been implicated in protein refolding or proteasomal degradation (for example, heat-shock proteins Hsp40, Hsp/Hsc70 (refs. 15,16) and CHIP[16]). To search for more proteins that interact with mutant SOD1, we performed yeast two-hybrid screening of a cDNA library from the total spinal cord of presymptomatic transgenic mice expressing the G93A SOD1 mutation (in which a glycine residue is replaced by an alanine residue). We discovered that chromogranins are interacting partners with mutant forms of SOD1, but not wild-type SOD1. The chromogranins, namely chromogranin-A (CgA) and chromogranin-B (CgB), are soluble, acidic glycophosphoproteins and are major constituents of secretory large dense-core vesicles (LDCV) in neurons and endocrine cells. LDCV store neuropeptides and hormones and show regulated exocytosis upon appropriate cellular stimulation[17]. Chromogranins are transported in the trans-Golgi network (TGN) and translocate at the periphery in an actin-dependent manner during their maturation process[18]. Although the physiological functions of chromogranins are still unclear, previous reports have shown that their proteolytic products function as antibiotics, regulators of hormone release, controllers of intracellular $Ca^{2+}$ concentration and protein sorting machineries[17]. The role of chromogranins in neurons is unknown. Both CgA and CgB proteins are transported in the rat sciatic

[1]Department of Anatomy and Physiology, Laval University, Centre de Recherche du Centre Hospitalier de l' Université Laval, 2705 boulevard Laurier, Sainte-Foy, Quebec G1V 4G2, Canada. [2]Department of Psychiatry, Centre de Recherche Université Laval Robert-Giffard, 2601 de la Canardiere, Quebec, Quebec G1J 2G3, Canada. [3]Laboratory for Structural Neuropathology and [4]Motor System Neurodegeneration, RIKEN Brain Science Institute, 2-1 Hirosawa, Wako, Saitama, 351-0198, Japan. Correspondence should be addressed to J.-P.J. (jean-pierre.julien@crchul.ulaval.ca).

Received 15 September; accepted 26 October; published online 20 December 2005; doi:10.1038/nn1603

nerve[19] and CgA is found in motor endplates in the diaphragm[20], suggesting a possible role in neurotransmission.

Previous evidence indicates that chromogranins are involved in neurodegenerative diseases. Immunohistochemical studies have revealed the presence of CgA or CgB in neuritic senile plaques of Alzheimer brains[21] and in prion protein deposits of Creutzfeldt-Jacob disease brains[22]. The staining pattern of CgA is also altered in motor neurons of people with sporadic ALS[23]. Importantly, there is evidence that CgA can activate microglia to produce various pro-inflammatory molecules such as tumor necrosis factor-alpha (TNF-α), nitric oxide and potential neurotoxins including glutamate and cathepsin B[24–26].

Here we report that CgA and CgB, which are abundant proteins in motor neurons and interneurons, may act as chaperone-like proteins to



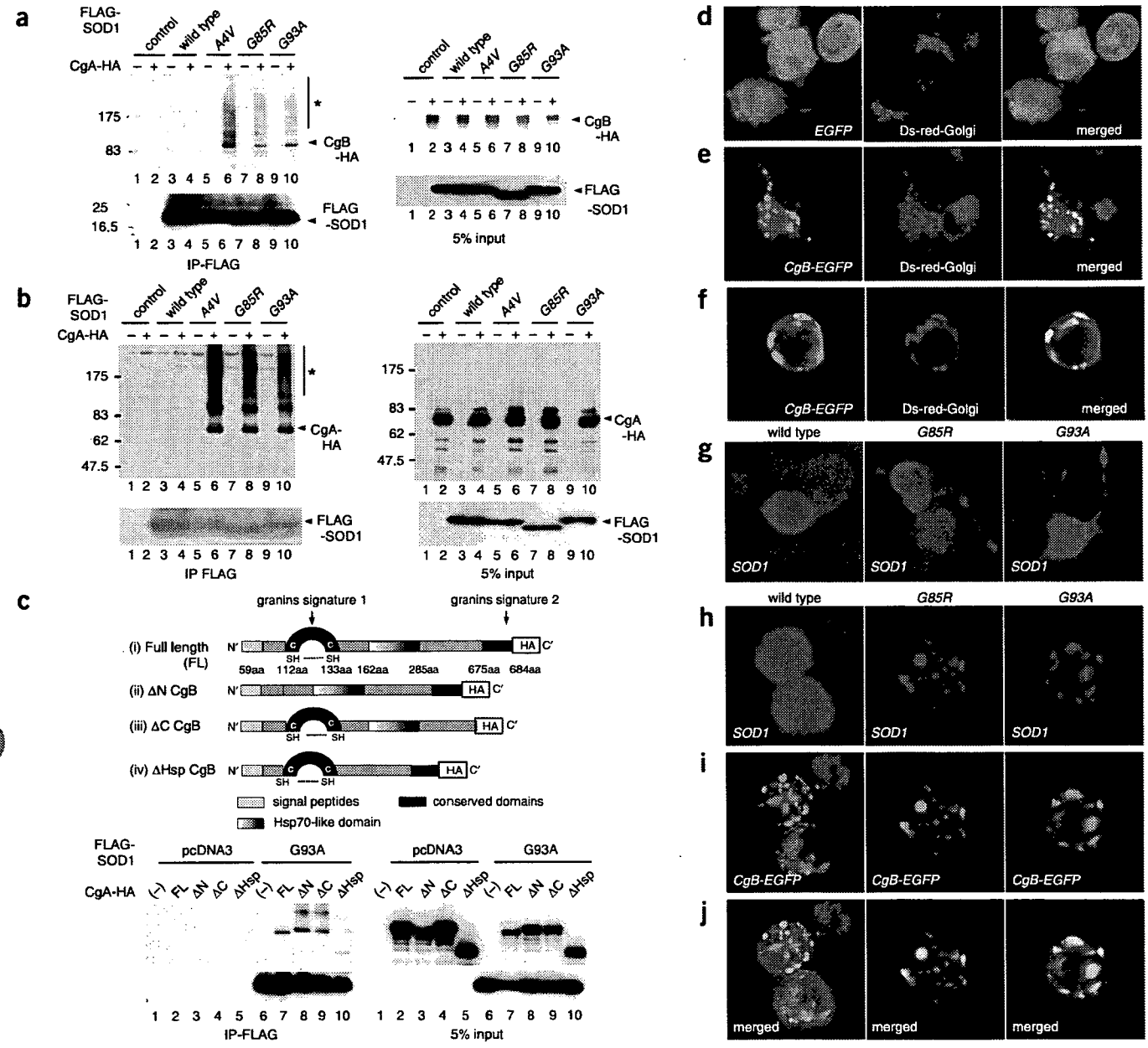


**Figure 1** Selective interactions of chromogranins with mutant SOD1 species but not with wild-type SOD1. (**a**,**b**) Chromogranins interact with mutant SOD1 in cultured cells. Neuro2a cells were transiently transfected with FLAG-tagged human *SOD1* (wild-type, A4V, G85R or G93A) and HA-tagged mouse CgB (**a**) or CgA (**b**). Immunoprecipitates with anti-FLAG affinity gel (IP-FLAG) and total cell lysates (5% input) were analyzed by western blotting using antibodies to SOD1 or HA. Note that both CgB and CgA immunoprecipitated with mutant SOD1 to yield high molecular weight species (asterisk). (**c**) An Hsp70-like domain in CgB interacts with mutant SOD1. Schematic representation of full-length (FL) or deletion mutants (N terminus (ΔN), C terminus (ΔC) or Hsp70-like domain (ΔHsp)) of CgB (top). Total cell lysates and immunoprecipitates from Neuro2a cells transfected with *FLAG-SOD1* or full-length *CgB* (FL) or its deletion mutants (ΔN, ΔC, ΔHsp) were analyzed by western blotting using the same antibodies (bottom). (**d–f**) Localization of CgB in the TGN of transfected Neuro2a cells. Images show live cells from confocal laser microscope of Neuro2a cells transfected with a plasmid encoding Ds-Red and a Golgi marker (*Ds-Red-Golgi*, middle) and EGFP (**d**) or EGFP-fused CgB (*CgB-EGFP*, **e** and **f**). (**g–j**) Overexpressed SOD1 mutants localized with CgB in the TGN of Neuro2a cells. Neuro2a cells were transiently transfected with human SOD1 (wild-type, G85R and G93A) together with (**i–k**) or without (**h**) CgB-EGFP, and analyzed by immunocytochemistry using mouse monoclonal anti-SOD1.

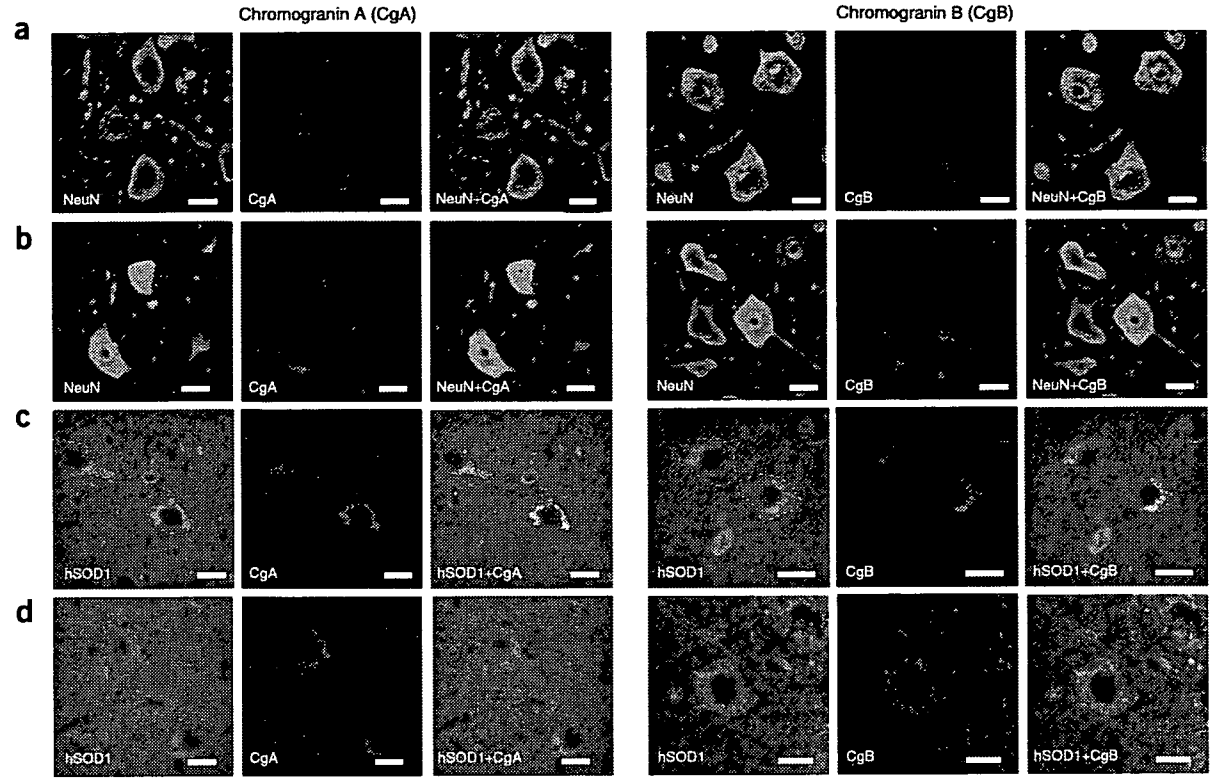


**Figure 2** Expression pattern of chromogranins in *SOD1* transgenic mice. We used the lumbar spinal cords from (**a**) nontransgenic littermates, (**b,c**) transgenic mice at 7 months of age and (**d**) transgenic mice at 9 months of age. The transgenic mice expressed either G37R *SOD1* (**b,c**) or wild-type *SOD1* (**d**). The following combinations of antibody stains were used: (**a,b**) mouse monoclonal anti-NeuN plus rabbit polyclonal anti-CgA (left) or anti-CgB (right); (**c,d**) sheep polyclonal antibody specific to human SOD1 plus anti-CgA (left) or anti-CgB (right). In **c**, the dotted lines demarcate the cell body of motor neurons. Scale bars, 50 μm.



promote secretion of misfolded SOD1 mutants. Moreover, our results demonstrate that extracellular mutant SOD1 can induce microgliosis and motor neuron death, suggesting that the chromogranin-mediated secretion of mutant SOD1 proteins could be a pathogenic mechanism in ALS. This idea is consistent with findings that the disease is not strictly autonomous to motor neurons and that toxicity is transferable from one cell to another.

## RESULTS

### Interaction of CgA and CgB with mutant SOD1 in cultured cells

To identify new proteins that interact with mutant SOD1, we used a yeast two-hybrid approach to screen a cDNA library from the spinal cord of pre-symptomatic mice transgenic for human G93A *SOD1*, using monomeric LexA-human G93A SOD1 as bait. As expected, the majority of the 250 surviving clones expressed human SOD1 that can dimerize with the bait. However, we obtained one clone whose sequence corresponded to a partial mouse CgB sequence encoding 76 amino acids. A full-length mouse CgB clone was then isolated from a brain cDNA library of C57Bl/6 mice and used as bait in the yeast two-hybrid system to confirm a specific interaction of CgB with mutant SOD1, but not with wild-type SOD1 (data not shown). To further investigate the interaction of CgB with mutant forms of SOD1 in a mammalian cell system, we carried out transient coexpression assays with Neuro2a cells using plasmid vectors coding for CgB tagged with hemagglutinin (HA) at the carboxy (C) terminus and for various human SOD1 species tagged with FLAG at the amino (N) terminus. We tested various SOD1 mutants, including the A4V, G85R and G93A mutants, to confirm that chromogranins interact with misfolded SOD1 mutants in general, not just the G93A mutant. As shown in pull-down assays (**Fig. 1a**), CgB was co-immunoprecipitated with mutant forms of SOD1, but not with wild-type SOD1. Pull-down assays revealed that CgA, another member of the mouse chromogranin family, also associated with SOD1 mutants but not with wild-type SOD1 (**Fig. 1b**). Similar results were obtained with human chromogranins (data not shown).

CgA and CgB share two conserved domains near their N and C termini, named the granin domains. The N-terminal granin domain is implicated in a sorting mechanism[27], whereas the C-terminal granin domain is necessary for dimerization or tetramerization of chromogranins[28]. To determine the CgB region responsible for interaction with mutant SOD1, we constructed expression plasmids for CgB mutants lacking specific domains and transiently expressed them together with mutant SOD1 into Neuro2a cells (**Fig. 1c**, top). An immunoprecipitation experiment showed that CgB mutants with deleted granin domains (ΔN or ΔC) were still able to interact with mutant SOD1 (**Fig. 1c**, bottom). A search for sequence homologies revealed that both CgB and CgA contain internal sequences with homologies to the substrate-binding site of mammalian Hsp70 (**Supplementary Fig. 1** online). A CgB mutant lacking this internal region (ΔHsp) did not bind mutant SOD1, as determined by the pull-down assay (**Fig. 1c**). The presence of an Hsp70-like domain offers a reasonable explanation for the specific binding of chromogranins to misfolded SOD1 mutants and not to wild-type SOD1.

Confocal microscopy of transfected Neuro2a cells provided further evidence of interactions between SOD1 mutants and chromogranins. Transfection of a construct encoding CgB fused at the C terminus to

enhanced green fluorescent protein (EGFP) (*CgB-EGFP*) into Neuro2a cells showed CgB accumulation in the TGN, as indicated by colocalization with Ds-Red fused to the Golgi-targeting human β1,4-galactoysltransferase (Ds-Red-Golgi) (**Fig. 1d–f**). Unlike chromogranins, SOD1 is a cytosolic protein without signal peptide and it is synthesized in free ribosomes. As expected, wild-type SOD1 yielded a cytosolic distribution when overexpressed in Neuro2a cells, and the expression of CgB had no effect on its distribution (**Fig. 1g–j**, left). In contrast, the subcellular distribution of mutant SOD1 species (G85R or G93A) was altered by the overexpression of CgB. A total colocalization of mutant SOD1 with CgB was observed in roughly 10% of doubly transfected Neuro2a cells (**Fig. 1g–j**, middle and right). These results indicate that CgB can influence the subcellular distribution of SOD1 mutants under the condition of overexpression in cultured cells.

### Colocalization of mutant SOD1 and CgA/B *in vivo*

We confirmed by *in situ* hybridization that CgA and CgB are expressed throughout the gray matter of spinal cord in mice, in motor neurons, interneurons and dorsal neurons. Immunohistochemistry showed that both CgA and CgB are more predominantly detected in dorsal neurons and interneurons than in motor neurons (**Supplementary Fig. 2** online), which is consistent with previous reports[29,30].

Immunofluorescence microscopy showed that CgA and CgB are located in perinuclear vesicles in the spinal motor neurons of normal mice stained by anti-NeuN antibody (**Fig. 2a**). In presymptomatic *G37R SOD1* mice (7 months old), perinuclear vesicles labeled by antibody to CgA or CgB were deformed and fused together (**Fig. 2b**), possibly reflecting damage to the Golgi apparatus[31]. We also detected partial colocalization of mutant SOD1 with CgA and CgB in irregular and large vesicular structures of spinal neurons from *G37R SOD1* transgenic mice (**Fig. 2c**). In the *SOD1* (wild-type) transgenic mice, the distribution patterns of CgA and CgB were similar to those of nontransgenic mice with no obvious colocalization between wild-type SOD1 and chromogranins (**Fig. 2d**).

To confirm the distribution of mutant SOD1 in the endoplasmic reticulum (ER)-Golgi system, we carried out subcellular fractionation of spinal cord lysates from transgenic mice expressing wild-type SOD1 or G37R SOD1 at different ages. Western blot analysis clearly demonstrated that mutant SOD1 was recovered in both heavy and light membrane fractions containing mitochondria and microsomes (**Fig. 3a**). The calculation from the densitometric value of SOD1 monomer revealed that, in the preclinical stage (6 months old), 23.6% of G37R SOD1 was found in heavy membrane fractions, and 4.2% in light membrane fractions. For wild-type SOD1, 13.4% was found in heavy membrane fractions and 1.91% in light membrane fractions. After paralysis, 6.46% of monomeric G37R SOD1 accumulated in the light membrane

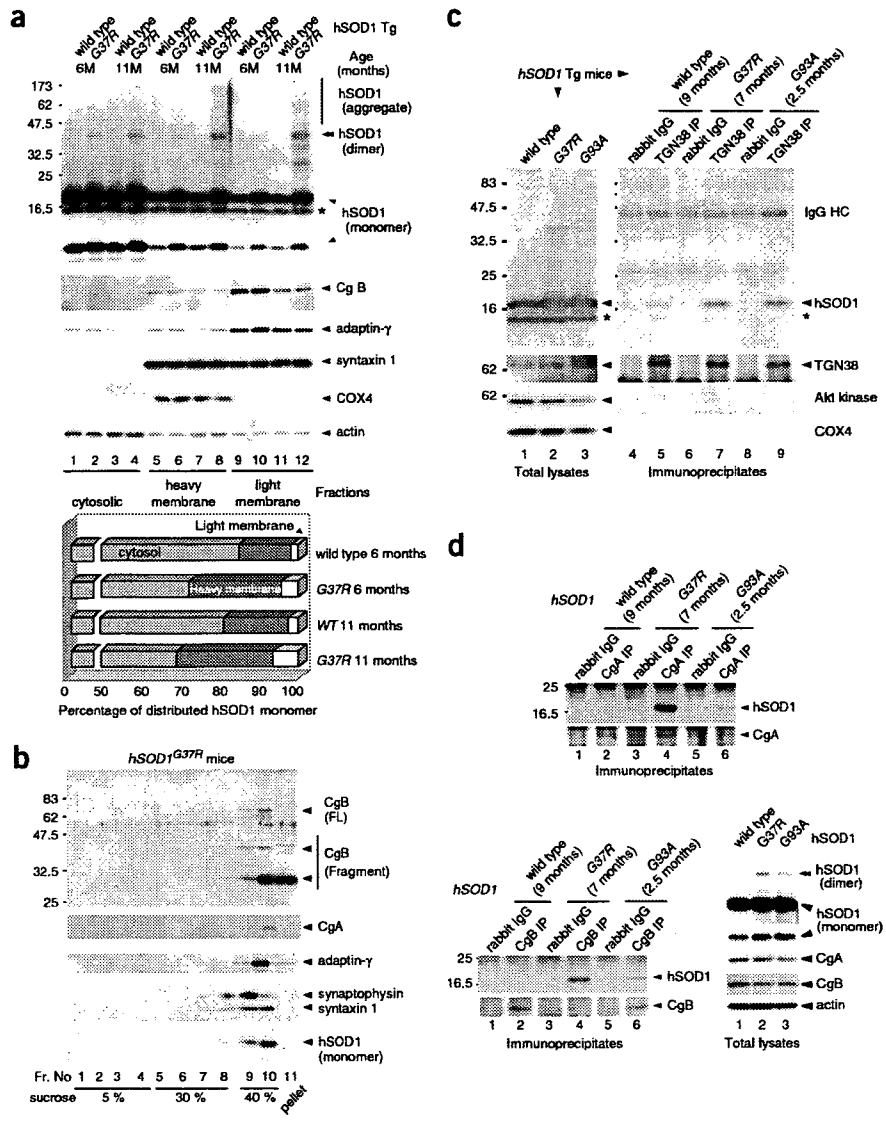


**Figure 3** SOD1 mutants in spinal cord of ALS mice accumulate in TGN and co-immunoprecipitate with chromogranins. (**a**) G37R SOD1 accumulated in both heavy and light membrane fractions. Subcellularly fractionated proteins from spinal cord of wild-type and G37R *SOD1* transgenic mice (6 and 11 months old) was analyzed by western blotting using antibodies specific to human SOD1, CgB, adaptin-γ, syntaxin-1, COX4 and actin. Asterisk indicates endogenous mouse SOD1. The percentage of monomeric human SOD1 in each fraction was presented from the densitometric value of monomeric SOD1 in the cytosolic, heavy and light membrane fractions that was standardized by actin, COX4 and syntaxin-1, respectively (bottom). (**b**) Fractionation of microsome components by sucrose density-gradient ultracentrifugation showing that G37R SOD1 co-distributed with CgA, CgB, adaptin-γ and syntaxin-1. The light membrane fraction from spinal cord of G37R *SOD1* transgenic mice (7 months old) was analyzed. (**c**) Distribution of SOD1 mutants in the TGN. The spinal cord lysates from transgenic mice expressing human wild-type *SOD1* (9 months), G37R (7 months) or G93A (3 months) *SOD1* were immunoprecipitated with rabbit polyclonal anti-TGN38 preincubated with Protein G magnetic beads. The total tissue lysates and immunoprecipitates were analyzed by western blotting with antibodies to human SOD1, TGN38, Akt kinase and COX4. (**d**) Pull-down assay showing that CgA and CgB interacted with mutant SOD1 but not wild-type SOD1 in human SOD1 transgenic mice (wild-type, G37R and G93A). Spinal cord lysates were immunoprecipitated with anti-CgA or anti-CgB, which was analyzed using antibody to human SOD1.